

# ‘Anomalous’ magnetic fabrics of dikes in the stable single domain/superparamagnetic threshold

Carles Soriano,<sup>1</sup> Elisabet Beamud,<sup>2</sup> Miguel Garcés<sup>3</sup> and Michael H. Ort<sup>4</sup>

<sup>1</sup>Institut de Ciències de la Terra Jaume Almera (ICTJA), Consejo Superior de Investigaciones Científicas (CSIC), c/Lluís Solé Sabarís s/n, E-08028 Barcelona, Spain. E-mail: csoriano@ictja.csic.es

<sup>2</sup>Laboratori de Paleomagnetisme Centres Científics i Tecnològics de la Universitat de Barcelona-ICTJA CSIC, c/Lluís Solé Sabarís s/n, E-08028 Barcelona, Spain

<sup>3</sup>Departament d'Estratigrafia Paleontologia i Geociències Marines, Universitat de Barcelona, c/Martí i Franquès s/n, E-08028 Barcelona, Spain

<sup>4</sup>School of Earth Sciences and Environmental Sustainability, Northern Arizona University, Flagstaff AZ 86011, USA

Accepted 2015 November 11. Received 2015 November 10; in original form 2015 April 23

## SUMMARY

‘Anomalous’ magnetic fabrics in dikes that appear to indicate flow into the wall confound many workers. Here, we present extensive magnetic data on five dikes from Tenerife, Canary Islands, and use these to interpret the causes of the anomalous fabrics. Comparison of the anisotropy of magnetic susceptibility (AMS) and anhysteretic magnetization (AARM) results show that, in some cases, the anomalous fabrics are caused by single-domain grains, which produce AMS fabrics perpendicular to the grain elongation, whereas AARM fabrics are parallel. To check this, hysteresis experiments were used to characterize the domain state. These show most are mixtures of pseudo-single-domain or single-domain plus multi-domain particles, but many have wasp-waisted hysteresis loops, likely indicating mixed populations of stable single-domain and superparamagnetic grains. First-order reversal curves were used to better characterize this and show mixtures of stable single-domain and superparamagnetic grains dominate the magnetic signal. Magnetic particles at the stable single-domain/superparamagnetic threshold are unstable at timespans relevant to the analytical techniques, so they produce complicated results. This suggests that anomalous AMS fabrics in dikes cannot simply be attributed to elongated stable single-domain particles and that mixtures of the different grain types can produce hybrid fabrics, in which the fabrics are neither perpendicular or parallel to the dike plane, that are difficult to interpret without extensive magnetic analysis.

**Key words:** Magnetic fabrics and anisotropy; Physics of magma and magma bodies; Effusive volcanism.

## 1 INTRODUCTION

The anisotropy of magnetic susceptibility (AMS) is the most widely used method to infer magma flow in dikes. It has been applied to rocks of all ages in the geological record, which include a wide variety of geodynamic settings and magma compositions. The interpretation of magma flow in dikes using AMS data has been systematically improved since the pioneer works by Khan (1962) and Ellwood (1978). Early interpretations of magma flow relied on the assumption that AMS fabric is flow related if the maximum susceptibility axes ( $K_1$ ) are in, or imbricate to, the dike plane (Knight & Walker 1988; Ernst & Baragar 1992; Tauxe *et al.* 1998). More recent studies emphasize that interpretation of magma flow should be based on the shape of the AMS fabric and suggest that, for planar fabrics, the plane of magnetic foliation is a more suitable indicator of magma flow than  $K_1$  (Geoffroy *et al.* 2002; Callot & Guichet 2003; Porreca *et al.* 2006; Delcamp *et al.* 2014).

In any study of the AMS in dikes, there are a number of possible fabrics whose interpretation in terms of magma flow is not straightforward. These fabrics are currently termed ‘anomalous’ or ‘abnormal’, as opposed to ‘normal’ fabrics, which allow for a more straightforward interpretation. Table 1 illustrates the variability of anomalous and inverse fabrics with respect to flow-related fabrics as reported in some AMS studies in the literature. Dikes sampled along cross-section profiles reveal that anomalous and normal fabrics may coexist within a dike profile (Herrero-Bervera *et al.* 2001; Kissel *et al.* 2010). Inverse fabrics, a particular type of anomalous fabric in which the AMS fabric is oriented perpendicular to the dike plane, have been the subject of some debate and there is no current consensus on their interpretation and origin (Potter & Stephenson 1988; Rochette *et al.* 1999; Cañón-Tapia & Chávez-Álvarez 2004; Chadima *et al.* 2009; Hastie *et al.* 2011; Delcamp *et al.* 2014). In most cases, sites with such fabrics are discarded as not interpretable.

**Table 1.** Anomalous and inverse magnetic fabrics reported in studies of AMS in dikes.

Reference	N dikes	Anomalous	Inverse	Composition	Geologic context	Location
Delcamp <i>et al.</i> (2014)	79	19	12	Basalt	Ocean island rift zone	Tenerife
Chadima <i>et al.</i> (2009)	15	8	5	Basanite to trachybasalt	Intracontinental rift	Bohemian massif
Soriano <i>et al.</i> (2008)	89	19	2	Basalt to phonolite	Ocean island rift zone	Tenerife
Porreca <i>et al.</i> (2006)	16	6	3	Tephrite to phonolite	Stratovolcano	Vesubio
Poland <i>et al.</i> (2004)	2		0	Andesite/dacite	Stratovolcano	Colorado
Aubourg <i>et al.</i> (2002)	7		0	Rhyolite	Lava flow complex	Ponza
Callot <i>et al.</i> (2001)	8	5	3	Dolerite	Ocean spreading rift	Greenland
Raposo & D’Agrella-Filho (2000)	81	9	9	Basalt to andesite	Intracontinental rift	Brazil
Tauxe <i>et al.</i> (1998)	251	62	6	Basalt to andesite	Ophiolite complex	Cyprus
Rochette <i>et al.</i> (1991)	29	11	6	Basalt to andesite	Ophiolite complex	Oman
Knight and Walker (1988)	61	7	?	Basalt	Ocean island rift zone	Hawaii

The aim of this contribution is to improve the interpretation of AMS data in dikes by focusing on anomalous fabrics, in order to see if they can be used to infer magma flow in dikes. We study the magnetic properties along cross-section profiles in five dikes selected from rift zones of the Anaga massif, in the Miocene basaltic shield of Tenerife, Canary Islands. Soriano *et al.* (2008) provide details on the geologic setting and on the dike swarms in this rift zone. Silicate fabrics, magnetic fabrics, magnetic mineralogy and domain state are characterized for each particular dike with different techniques. The causes of anomalous fabrics are investigated for each dike and the domain state is believed to play a major role in inverse AMS fabrics and in the fabrics of the anisotropy of anhysteretic remanent magnetism (AARM). Based on our results, some implications for AMS studies and magma flow in dikes are highlighted.

## 2 FABRIC NOTATION AND SAMPLING PROCEDURE

Designation of a magnetic fabric as ‘anomalous’ is somewhat ambiguous and there is not a clear definition for the term. Anomalous fabrics include scattered AMS data on the stereoplot, different types of asymmetric fabrics with respect to the dike plane (for example ‘scissored’ fabrics), and inverse fabrics (Tauxe *et al.* 1998; Rochette *et al.* 1999; Borradaile & Gauthier 2003; Féménias *et al.* 2004; Chadima *et al.* 2009). In turn, designation of a magnetic fabric as ‘inverse’ depends on the criteria chosen to infer magma flow (magnetic foliation or magnetic lineation), which ultimately depends on the shape of the AMS ellipsoid. Scattered data on the stereoplot, asymmetric fabrics and inverse fabrics may have different causes. They can be sampling and/or data processing artefacts but can also correspond to physical phenomenon such as shearing, crystallization of magnetic minerals perpendicular to the dike walls and the relation between confining pressure and buoyant forces of magma.

In this work, we use a two-fold fabric notation based on the shape of the AMS ellipsoid. If the AMS ellipsoid is oblate, the magnetic fabric is considered as normal when the magnetic foliation ( $K_1$ – $K_2$  plane) is parallel or imbricated ( $\leq 35^\circ$ ) to the dike plane and it is considered as inverse when the magnetic foliation is perpendicular to the dike plane. If the AMS ellipsoid is prolate, the magnetic fabric is considered as normal when the magnetic lineation ( $K_1$ ) is parallel or imbricated ( $\leq 35^\circ$ ) to the dike plane and it is considered inverse when the magnetic lineation is perpendicular to the dike plane. For triaxial AMS ellipsoids we use the same criteria than for prolate AMS ellipsoids. To avoid ambiguity, we designate all other fabrics with descriptive terms (Table 2).

For this study, five dikes were sampled across profiles perpendicular to the dike margins. Dikes were selected based upon a previous study (Soriano *et al.* 2008). One dike has a normal fabric and the other four are classified as anomalous or inverse. The sampled dikes are basaltic to phonolitic and porphyritic, with euhedral pyroxene, plagioclase, olivine, amphibole and sanidine phenocrysts in a groundmass of plagioclase microlites. Opaque minerals occur in different proportions as phenocrysts and as small crystals in the groundmass. Dikes are subvertical and some are segmented. They range from 120 to 265 cm thick and intrude coherent lavas and autobreccias and other dikes of basaltic composition. Dikes show planar to wavy chilled margins up to 5 cm thick. Both dike margins are subparallel (Fig. 1). Dikes show columnar jointing perpendicular to dike margins and flow banding subparallel to the margins. In some cases, vesicles with oblate and prolate shapes are imbricated with respect to the margins (Table 2). Core samples were obtained with a portable drill and oriented with magnetic and sun compasses. About 30 cores were drilled for each dike, distributed in five groups of 6 cores: two groups on both margins within 10 cm of the dike walls, one group at the centre of the dike, and two groups at intermediate positions between the centre and the margins (Fig. 1). Individual cores were drilled as close as possible to others within their group, so that the 6 cores of each group are within a distance of less than 50 cm along the length of the dike.

## 3 METHODS

This study includes analysis of oriented thin sections on the optical and SEM microscopes, X-ray diffraction analyses (XRD), energy-dispersive X-ray spectroscopy (EDS), measurements of the AMS, the AARM and the anisotropy of isothermal remanent magnetization (AIRM), acquisition of isothermal remanent magnetization (IRM) and three-axes thermal demagnetization of the IRM, hysteresis loops and First Order Reversal Curves (FORCs). All experiments were conducted at room temperature.

A powder diffractometer Bruker-AXS D5005 was used at the Institute of Earth Sciences Jaume Almera (ICTJA CSIC) to conduct the XRD analyses of selected samples. Oriented thin sections were studied with a Zeiss DSM 940A scanning electron microscope and EDS detector at the Centres Científics i Tecnològics at the Universitat de Barcelona (CCiTUB).

AMS was measured with a Kappabridge KLY-2 (Geofyzika Brno) at the Laboratory of Palaeomagnetism of the CCiTUB - ICTJA CSIC following the 15-position scheme of Jelinek (1977). Data were processed with the Pmag software package developed by L. Tauxe (Pmag1.9 version) and the program ANISOFT4.2 (Agico).

Table 2. Field data and AMS fabric types of the studied dikes.

Dike	Latitude	Longitude	Dip direction	Dip (cm)	Composition	Host rock	Chilled margin	Structural features	Flow features	Cooling features	Vesicles	AMS fabric type
AD-10	N 28°31.649'	W 16°11.708'	113	74	Phonolitic	Basaltic dike	Planar/ondulated		Flow hinge at dike center	Columnar jointing		Normal
AB-4	N 28°31.731'	W 16°09.432'	249	83	Basaltic	Coherent lava	Planar			Columnar jointing		Inverse
AC-1	N 28°30.731'	W 16°11.529'	21	79	Basaltic	Coherent lava	Planar, 2 cm			Columnar jointing		Inverse, scattered
AD-6	N 28°30.365'	W 16°13.955'	135	78	Basaltic	Autobreccia	Wavy, 5 cm		Flow banding	Columnar jointing	Prolate	Inverse, scattered
AD-12	N 28°30.916'	W 16°13.988'	121	60	Phonotephritic	Coherent lava	Planar	Segmented dike		Columnar jointing	Oblate	Inverse, asymmetric

Whereas AMS summarizes the fabric caused by all magnetic contributions (dia-, para- and ferromagnetic minerals), AARM and AIRM reflect the anisotropy component due only to the orientation of remanence-bearing minerals (Cox & Doell 1967; McCabe *et al.* 1985; Jackson 1991). AIRM and AARM analyses were carried out on a few samples at the Alpine Laboratory of Palaeomagnetism (ALP) in order to choose the best technique to study the anisotropy of remanence. Although both methods yielded similar results, AIRM data were more scattered. Hence, AARM was the method chosen to perform measurements on samples from those groups of cores showing inverse AMS fabric and also on samples from groups of cores with normal, scattered and asymmetric AMS fabrics. AARM measurements were not intended to yield quantitative estimations of the AARM fabrics but just to investigate the coaxiality between AMS and AARM fabric axes. For these reason AARM experiments were conducted only on three to four samples of each group of cores. AARM was obtained after applying an ARM in either 6 or 12 different positions with AF of 60 mT and DC of 100  $\mu$ T. Between each position, specimens were demagnetized by AF tumbling with a Molspin AF demagnetizer. Computation of the AARM tensor was done with the program AREF (v2.0; Agico).

IRM acquisition and three-axes stepwise thermal demagnetization experiments (Lowrie 1990) were performed on 46 samples across dike profiles. An impulse magnetizer IM10-30 (ASC Scientific) and a thermal demagnetizer TSD-1 (Schonsdted) at the Laboratory of Palaeomagnetism of the CCiTUB - ICTJA CSIC were used for these purposes. IRM acquisition began with a field of 500 mT imparted along the  $-Z$ -axis and subsequent increasing fields, from 1 to 500 mT, were applied along the  $+Z$ -axis in order to obtain the coercivity of remanence (Hcr). An IRM was successively imparted along three orthogonal axes of the sample (first 1.2 T along the  $Z$ -axis, then 0.3 T along the  $Y$ -axis and finally 0.1 T along the  $X$ -axis), followed by stepwise thermal demagnetization to obtain the unblocking temperature for each axis.

Hysteresis measurements were carried out with a MPMS XL SQUID magnetometer (Quantum Design) in the Magnetic Measurements Laboratory of the CCiTUB. The hysteresis loops were obtained by applying increasing fields from  $-2$  to  $+2$  T. The standard hysteresis parameters  $M_r$ ,  $M_s$ ,  $H_c$  and  $H_{cr}$ , where  $M_r$  is the saturation remanence,  $M_s$  is the saturation magnetization,  $H_c$  is the coercive force and  $H_{cr}$  is the coercivity of remanence, were plotted as  $M_r/M_s$  and  $H_{cr}/H_c$  ratios in the Day diagram (Day *et al.* 1977). The Day plot is a standard tool to discriminate the domain state, which is attributed to grain size variations in samples with titanomagnetite and magnetite. However, interpretation of the hysteresis parameters in terms of domain state can be ambiguous and characterizing the contributions of the different grain sizes in the magnetic signal is not always possible (Roberts *et al.* 2000; Dunlop 2002; Muxworthy *et al.* 2005; Smirnov 2006). FORC distributions allow a more precise characterization of the domain state and for this reason FORC experiments were conducted on selected samples. In particular, density distributions of FORC diagrams allow characterizing magnetostatic interactions along the  $H_u$  axis and coercive force along the  $H_c$  axis (Roberts *et al.* 2000; Muxworthy *et al.* 2005; Smirnov 2006). FORCs were measured with a vibration magnetometer Micromag 3900 (Princeton Measurements Corporation) at the Centro Nacional de Investigación de la Evolución Humana (CENIEH). The saturating field was 5kOe with an averaging time of 100 ms, getting 111 FORC curves for each FORC diagram. FORC's processing was carried out using the FORCinel

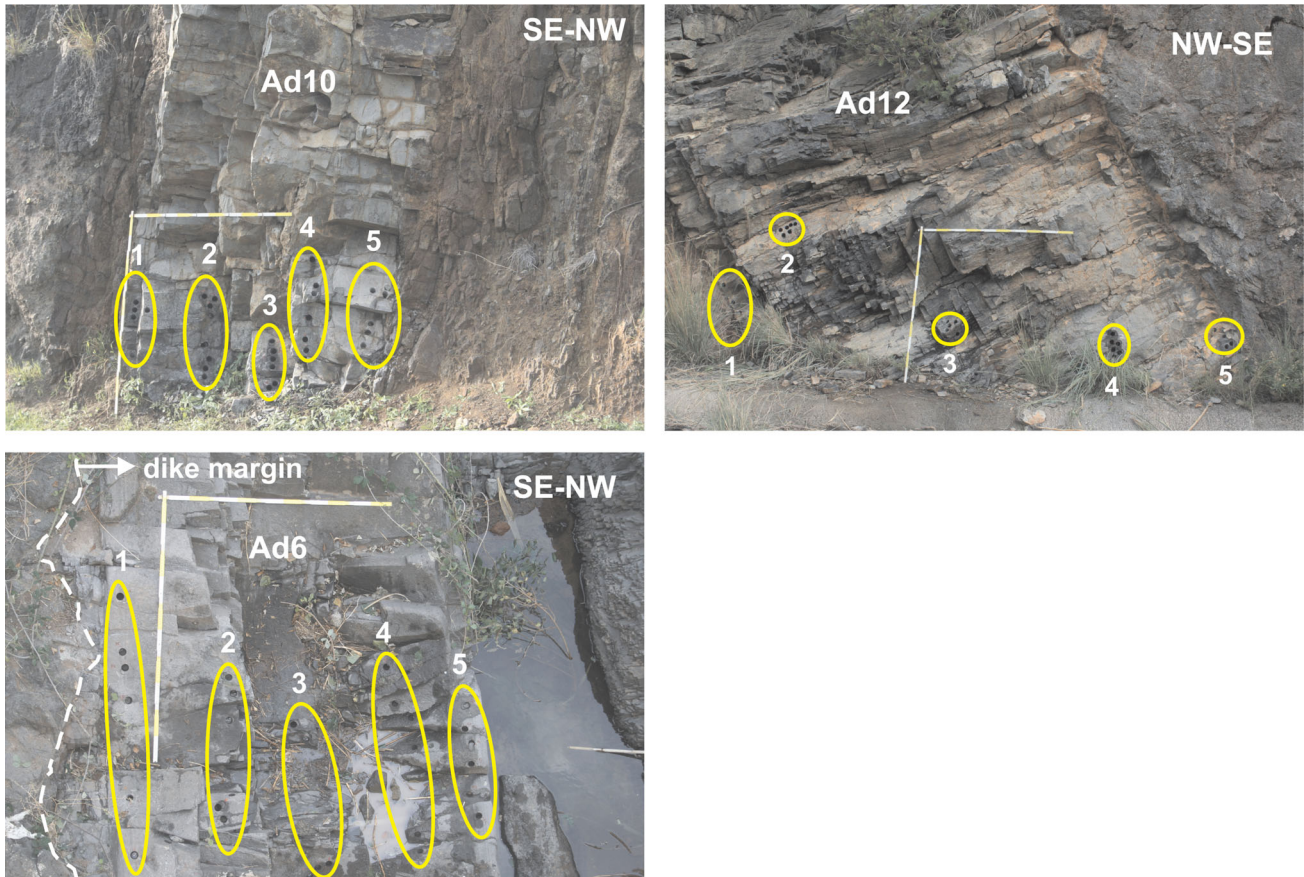


**Figure 1.** Photograph of dikes AD10, AD12 and AD6 showing the sampling strategy along cross-section profiles of dikes. 1 and 5 are groups of samples at dike margins, 3 is group of samples in dike centre and 2 and 4 are groups of samples in the intermediate positions.

and VARIFORC software packages (Harrison & Feinberg 2008; Egli 2013).

#### 4 MAGNETIC MINERALOGY

X-Ray diffraction analyses (XRD) indicate that the opaque minerals observed on the optical microscope are Fe–Ti oxides with an inverse spinel structure (Fig. 2). Energy-dispersive X-ray spectroscopy (EDS) of opaque minerals observed on the optical and SEM images show high contents of Ti and different amounts of Cr, Mg and Al, suggesting that opaque mineral are ulvospinel.

The measured IRMs show that dike rocks are fully saturated at 200 mT and that most of the IRM is acquired below 100 mT, which excludes antiferromagnetic minerals as carriers of the remanence (Fig. 3). Three-axis demagnetization curves show that most of the IRM is held in the soft coercivity fraction ( $<0.1$  T), with only some of the IRM held in the medium coercivity fraction (0.1–0.3 T), and that unblocking temperatures ( $T_b$ ) range from 550 to 300°C (Fig. 4). These results are consistent with titanomagnetite as the dominant magnetic carrier of remanence (Lowrie 1990; Roberts & Pillans 1993). Based on the unblocking temperatures, Ti substitution with respect to Fe in the titanomagnetite lattice of the studied dikes has been estimated to be 0.4 for AB4 ( $T_b \sim 300^\circ\text{C}$ ), 0.2 for AC1 and AD12 ( $T_b \sim 400^\circ\text{C}$ ) and close to 0.0 for dikes AD10 and AD6 ( $T_b \sim 550^\circ\text{C}$ ). IRM and three-axes stepwise thermal demagnetization were also investigated across dike profiles and suggest that variations in the magnetic mineralogy across profiles are negligible (Fig. 4b).

#### 5 PETROFABRICS OF DIKES

Thin sections perpendicular to the  $K_2$  axis of the AMS fabric were cut on cores oriented in the field. Overall, they show a fabric subparallel to the dike plane defined by prismatic pyroxene, amphibole, plagioclase and sanidine phenocrysts and by plagioclase microlites (Fig. 2). A few thin sections, generally corresponding to dike centres and to intermediate positions between the centre and the margins, show a poorly defined, nearly isotropic, fabric under thin section inspection. Fe–Ti oxides  $\geq 10 \mu\text{m}$  in diameter are either equant or skeletal grains and have no preferred orientation (Figs 2b and d). Dikes with inverse AMS fabric have acicular Fe–Ti oxides ( $\sim 10 \mu\text{m}$  length and  $\sim 1 \mu\text{m}$  width) organized in two subfabrics with different orientations. One fabric is subparallel to the silicate fabric and the other is normal to the silicate fabric (Fig. 2d). Amphibole phenocrysts of dike AD12 have equant ( $\leq 1 \mu\text{m}$  diameter) to elongated Fe–Ti oxides ( $5\text{--}7 \mu\text{m}$  length and  $\sim 2\text{--}3 \mu\text{m}$  width) distributed along chains separated about  $5 \mu\text{m}$ . The Fe–Ti oxides forming the chains are  $\leq 1 \mu\text{m}$  from each other. Chains of Fe–Ti oxides are typically subparallel to the silicate fabric of AD12 while the elongation of individual Fe–Ti oxides can be normal to the silicate fabric (Fig. 2f).

##### 5.1 Magnetic fabrics

AARM fabrics with principal axes at an angle  $\leq 20^\circ$  with respect to the AMS axes are considered as coaxial with the AMS fabric, the angular difference ascribed to instrumental error (AARM

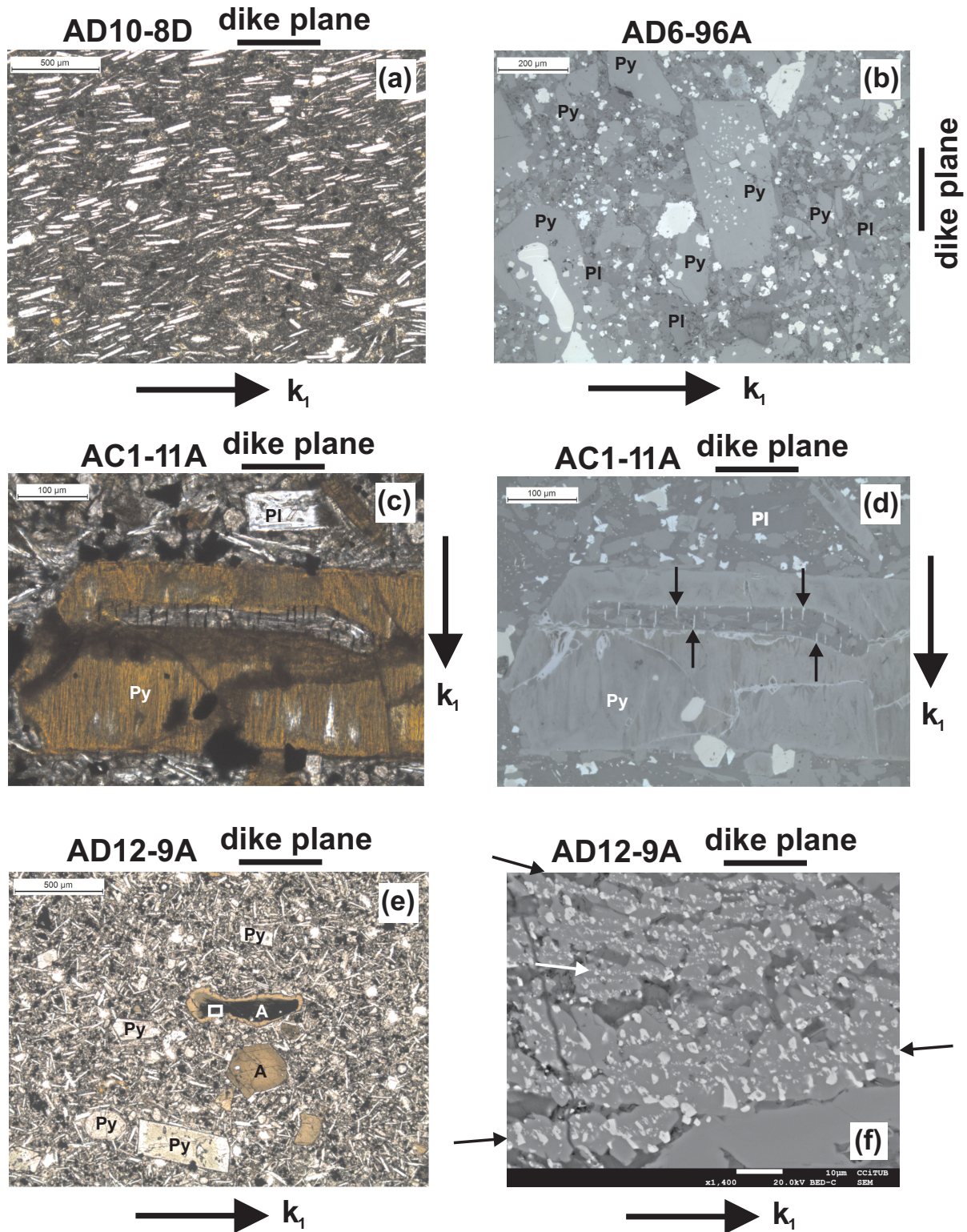


**Figure 2.** Oriented photomicrographs and Scanning Electron Microscope (SEM) image of the studied dikes. Black bar is the dike plane and arrow is  $K_1$  of the AMS ellipsoid. (a) Dike AD10 (cross-polarized light) with sanidine prismatic phenocrysts (white) oriented sub parallel to the dike plane and to  $K_1$ . (b) Dike AD6 (reflected light) with prismatic pyroxene (Py) and plagioclase (Pl) phenocrysts and skeletal Fe-Ti oxides (white). Phenocrysts are subparallel to the dike plane and normal to  $K_1$ . (c) Dike AC1 (cross-polarized light) with prismatic plagioclase phenocrysts (Pl), plagioclase microlites and a large pyroxene phenocryst (Py). Phenocrysts and microlites are subparallel to the dike plane and normal to  $K_1$ . (d) Dike AC1 (reflected light) showing acicular Fe-Ti oxides (white) parallel to  $K_1$  and normal to the silicate fabric and skeletal to equant Fe-Ti oxides (white). (e) Dike AD12 (plane-polarized light) with prismatic amphibole (A) and pyroxene (Py) phenocrysts and plagioclase microlites. Phenocrysts and microlites are dominantly subparallel to the dike plane and to  $K_1$ . (f) SEM image of the white rectangle on amphibole phenocryst in photomicrograph (e). Fe-Ti oxides (white) have shape anisotropy roughly normal to  $K_1$  and are distributed on amphibole phenocryst forming chains (arrows) subparallel to the dike plane and to  $K_1$ .

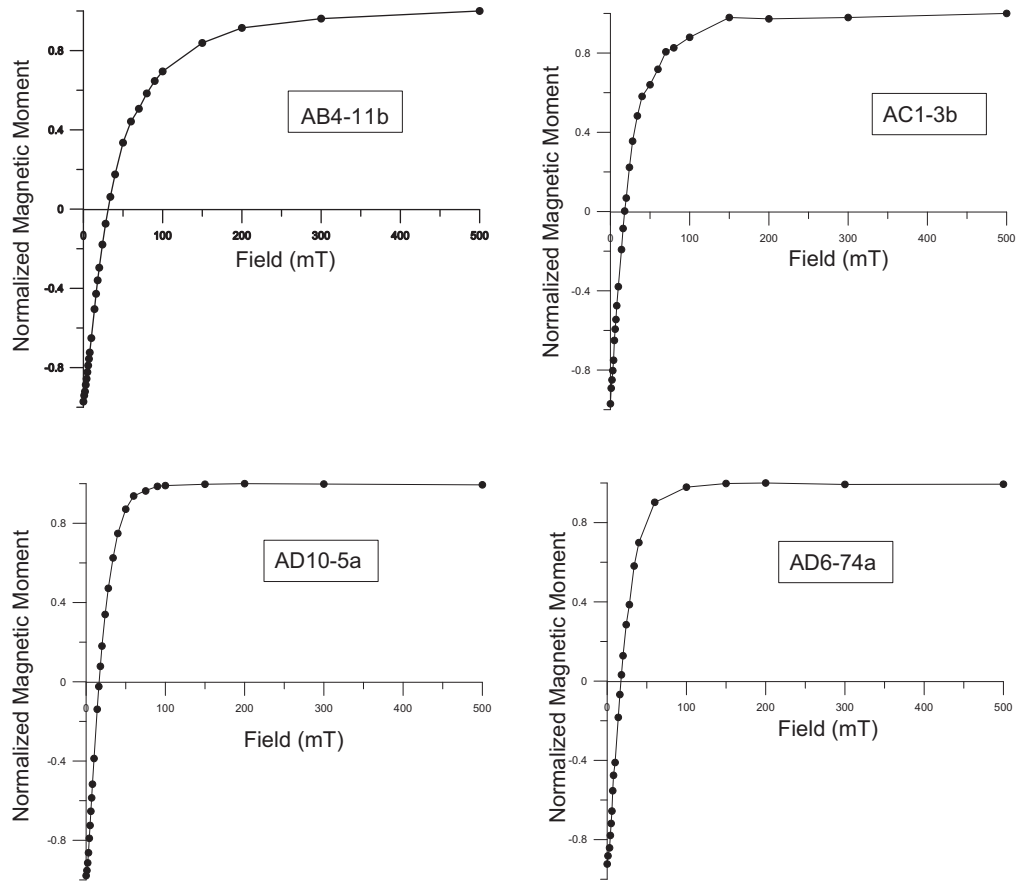


Figure 3. Acquisition of isothermal remanent magnetization (IRM) of selected samples along dike cross-section profiles.

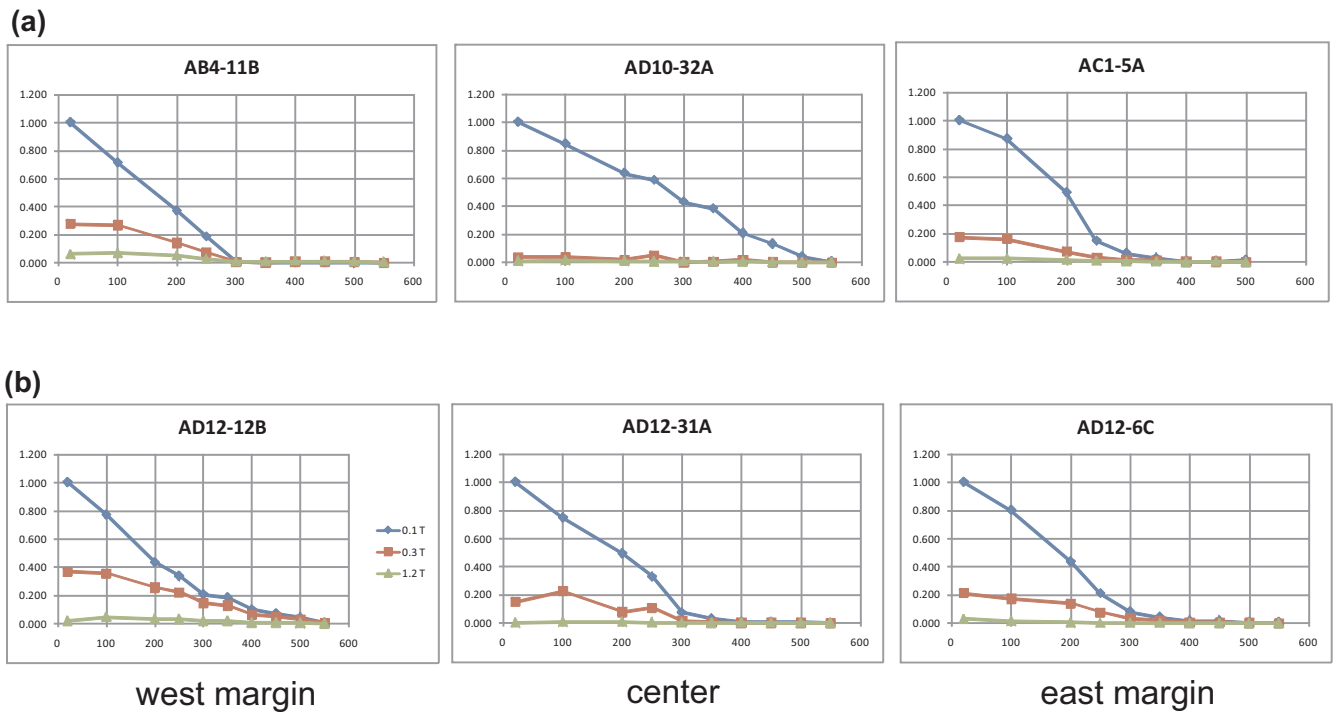
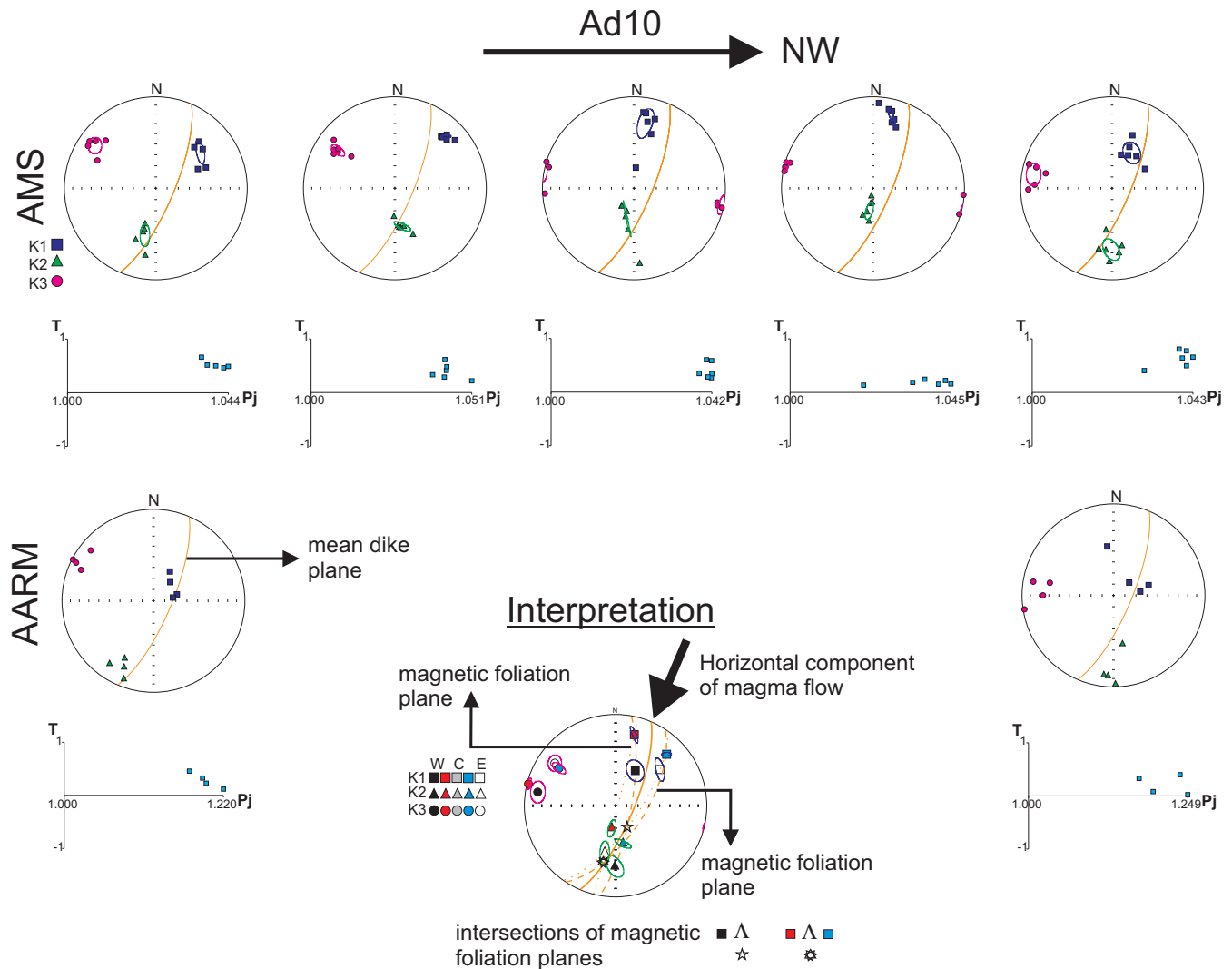


Figure 4. (a) Stepwise thermal demagnetization curves of IRM imparted along three orthogonal axes (1.2, 0.3 and 0.1 T fields) in selected samples of the studied dikes. (b) Stepwise thermal demagnetization of IRM along cross-section profile of dike AD12.



**Figure 5.** Equal-area lower-hemisphere stereograms of the principal AMS and AARM axes across profile of dike AD10. Diagrams of the corrected anisotropy degree ( $P'$ ) versus shape factor ( $T$ ) are shown for the AMS and the AARM. Interpretation of magma flow is based on the intersection of the magnetic foliation planes of the AMS (see text for discussion).

analyses have larger errors than AMS) and due to the absence of the paramagnetic contribution from the magnetic signal in the AARM measurements (Jackson 1991). Overall, AMS fabrics of all dikes are well grouped while AARM fabrics are more scattered and the anisotropy degree is higher for AARM fabrics than for AMS fabrics (Figs 5–9). Except AD10 (normal fabric), all the studied dikes show  $K_1$  axes of the AMS at nearly  $90^\circ$  to the dike plane (inverse fabric) in some parts of the dike profile and, in some cases, the AMS fabric is also asymmetric and scattered (Figs 5–9). The distribution of closely spaced Fe–Ti oxides along chains subparallel to the silicate fabric of dike AD12 suggest that magnetostatic interactions are significant in this dike and that distribution anisotropy of Fe–Ti oxides rather than their individual grain anisotropy controls the AMS (Hargraves *et al.* 1991; Stephenson 1994; Cañon-Tapia 1996).

Dike AD10 has a normal AMS fabric in which  $K_1$  imbricates on both margins and plunges about  $45^\circ$  to the NNE (Fig. 5).  $K_1$  of samples in the intermediate positions between the centre and the margins imbricate too and plunge shallower ( $\sim 20^\circ$ ) to the NNE. The AMS and AARM fabric ellipsoids are oblate and the AMS ellipsoid varies across the dike profile, being slightly more oblate at the margins than at the centre and in the intermediate positions.

AARM axes of samples from the dike margins are well grouped and parallel to the AMS axes, although  $K_1$  axes of AARM do not imbricate with respect to the dike plane and are about  $20^\circ$  steeper than  $K_1$  axes of AMS (Fig. 5).

Dike AB4 has an inverse AMS fabric on both margins while  $K_1$  axes are nearly in the dike plane the intermediate positions. The AMS fabric in the dike centre is quite dispersed (Fig. 6). The AMS ellipsoid is triaxial in the dike centre and is increasingly prolate towards the intermediate positions and towards both margins. The anisotropy degree ( $P'$ ) is among the highest of the studied dikes and does not show any clear trend across profile. The AARM fabric in the east margin and in the intermediate positions is nearly coaxial to the AMS fabric (Fig. 6). In the east margin,  $K_1$  axes of the AARM are well grouped and subhorizontal, forming an angle of  $20^\circ$  with respect to the subhorizontal  $K_1$  axes of the AMS. In the west margin,  $K_1$  axes of AARM are dispersed and closer to the dike plane than  $K_1$  axes of AMS, which are perpendicular to it.

Dike AC1 has an inverse AMS fabric on both margins with  $K_1$  at  $90^\circ$  to the dike plane (Fig. 7). In the dike centre and in the intermediate position between the centre and the west margin,  $K_1$  axes of the AMS are distributed on two clusters: three samples are

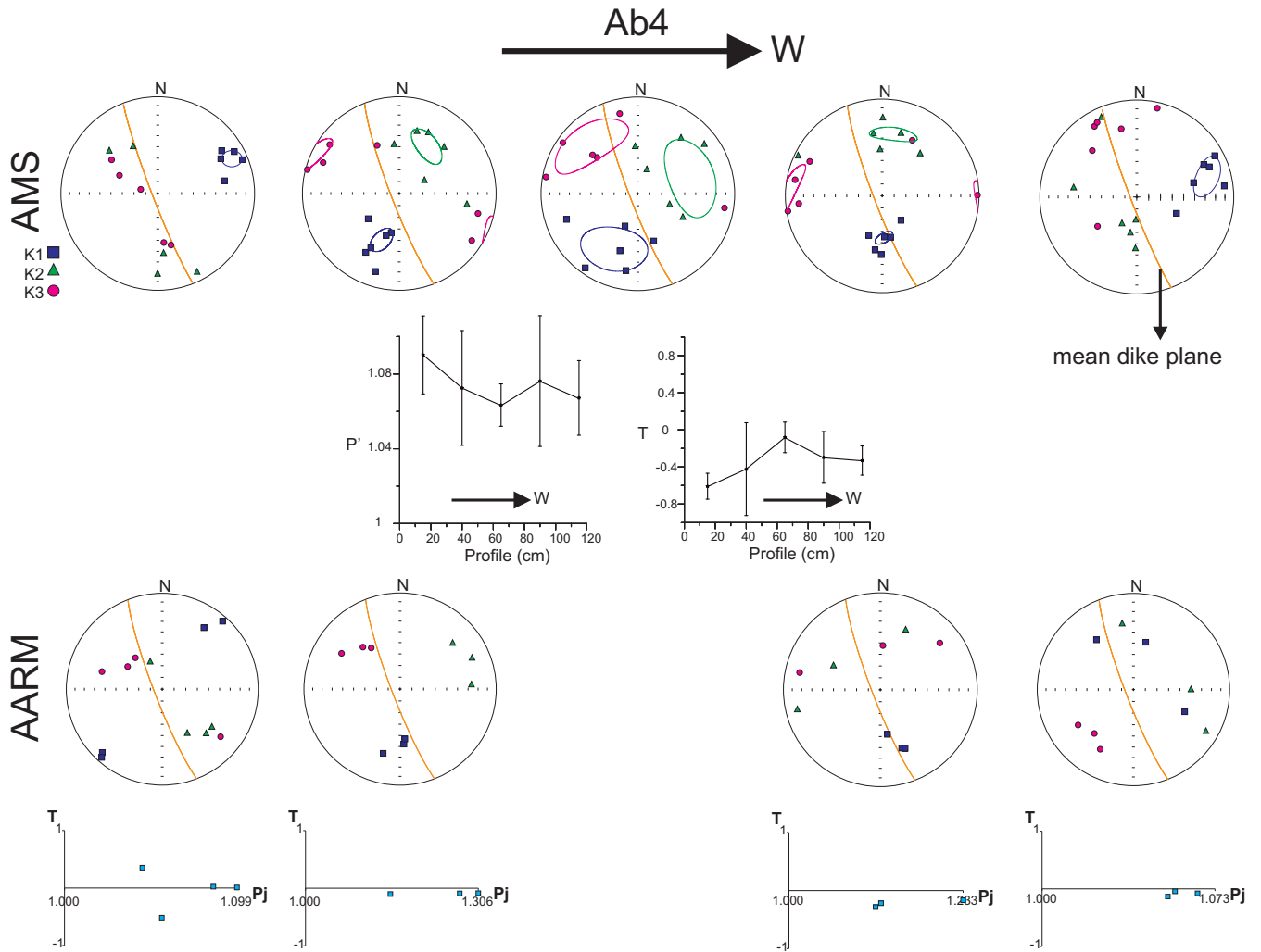


**Figure 6.** Equal-area lower-hemisphere stereograms of the principal AMS and AARM axes across profile of dike AB4. Variation across profile of the corrected anisotropy degree ( $P'$ ) and the shape factor ( $T$ ) is shown for the AMS and diagrams of the corrected anisotropy degree ( $P'$ ) versus shape factor ( $T$ ) are shown for the AARM.

nearly on the dike plane while the other three are perpendicular to it. In the intermediate position between the centre and the east margin,  $K_1$  axes of AMS form an angle of about  $30^\circ$  to the dike plane. The AMS ellipsoid is dominantly prolate, with the maximum 'prolateness' achieved on both margins (Fig. 7). Nevertheless, some samples of the east margin, the intermediate positions, and the centre are triaxial and slightly oblate. In the dike centre and the intermediate positions, the AARM fabric is more dispersed but roughly coaxial to the AMS fabric. In the east margin,  $K_1$  axes of the AARM are distributed along the dike plane while  $K_1$  axes of the AMS are well grouped and perpendicular to it. In the west margin,  $K_1$  axes of the AARM are closer to the dike plane than  $K_1$  axes of the AMS and form an angle of about  $45^\circ$  to  $K_1$  axes of the AMS (Fig. 7).

Dike AD6 has a well-defined flow foliation except in the 20 cm near the margins, and the dike walls are wavy and irregular (Fig. 1). The AMS fabric is somewhat scattered on both margins while it is well grouped and inverse in the rest of the dike profile (Fig. 8). The AMS ellipsoid of this dike is prolate on average although some samples are triaxial and oblate. The AARM fabric is somewhat dispersed. Overall,  $K_1$  axes of the AARM are closer to the dike plane than  $K_1$  axes of the AMS and form an angle  $>50^\circ$  to the

AMS axes. Nevertheless, a few samples of the AARM have  $K_1$  axes forming an angle  $\leq 20^\circ$  to the  $K_1$  axes of the AMS and can be considered as coaxial and parallel (Fig. 8).

Dike AD12 is a segmented dike with an asymmetric AMS fabric and a well-defined prolate AMS ellipsoid (Fig. 9). Asymmetry of the AMS fabric consists of  $K_1$  axes plunging to the N and NW while the dike plane dips steeply to the SE. The angular relations between  $K_1$  axes and the dike plane become clearer when data are rotated to dike coordinates (Fig. 9).  $K_1$  is gradually more perpendicular to the dike plane when moving from the east margin to the dike centre and to the intermediate position between the centre and the west margin. In the west margin,  $K_1$  forms an angle of about  $2^\circ$  to the dike plane. The AARM fabric is scattered and the shape ellipsoid is not well-defined (Fig. 9).

### 5.2 Magma flow features inferred from magnetic fabrics

The AMS fabrics of some of the studied dikes can be interpreted in terms of magma flow. Dike AD10 allows a straightforward interpretation of the magma flow vector. Because the shape of the AMS ellipsoid is oblate, we use the plane of the magnetic foliation

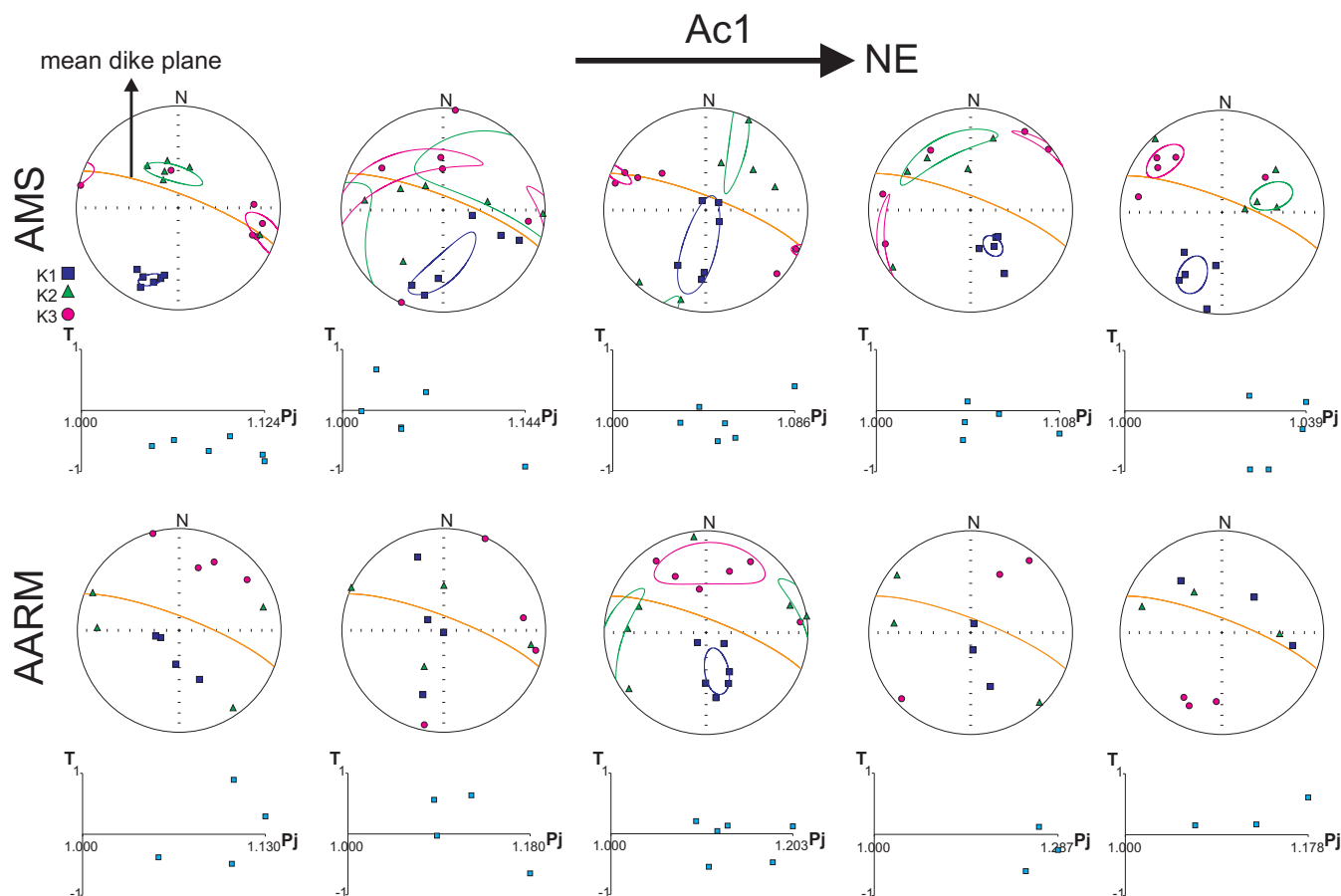


**Figure 7.** Equal-area lower-hemisphere stereograms of the principal AMS and AARM axes across profile of dike AC1. Diagrams of the corrected anisotropy degree ( $P_j$ ) versus shape factor ( $T$ ) are shown for the AMS and the AARM.

as a flow indicator (Geoffroy *et al.* 2002). The intersections of the magnetic foliation planes at both margins and at the intermediate positions are on the dike plane (Fig. 5). The intersection at both margins plunges steeply to the SSE while the intersection at the intermediate positions plunges shallower to the SSW. Hence, magma flow is directed to the SSW and is shallower at the margins than in the intermediate positions. Notably, using  $K_1$  as flow indicator would give a different interpretation of the evolution of magma flow during intrusion: a steeper flow vector would result on the margins and a shallower one in the intermediate positions (Fig. 5).

Dike AB4 has a dispersed AMS fabric and triaxial ellipsoid in the dike centre, which can be interpreted as poorly defined shear in stagnant magma in the dike centre. Dike AD6 has a scattered AMS fabric on the margins, which may arise from a poorly defined shear and dispersion of the magma flow vector, an interpretation reinforced by observations of irregularities of the dike borders and poorly defined flow foliation close to the margins (Fig. 1).

The AMS of dike AD12 is likely controlled by distribution of Fe–Ti oxides subparallel to the silicate fabric and regardless of the cause of the AMS it results from physical rock fabric (Hargraves *et al.* 1991; Stephenson 1994). Dike segmentation and asymmetric AMS fabric of dike AD12 suggest that this dike has been intruded under shear stress (Correa-Gomes *et al.* 2001; Féménias *et al.* 2004; Soriano *et al.* 2007; Eriksson *et al.* 2014). The magma flow vector and the shear vector resolved on the dike plane during intrusion are not known. Nevertheless, based on the fabric asymmetry and on the theoretical models proposed by Correa-Gomes *et al.* (2001) and

Soriano *et al.* (2007), the flow vector and the shear vector can be inferred. Magma flow is oblique and directed upward to the SSW while the shear vector is clockwise and subparallel to the flow vector (Fig. 9).

## 6 DOMAIN STATE

Inverse AMS fabrics can be caused by stable single-domain (SSD) magnetite (Potter & Stephenson 1988), so a first step when investigating the origin of inverse AMS fabrics is to characterize the domain state. We investigated the domain state of selected samples by means of hysteresis experiments (Suppl. file #1). The high field slope of the hysteresis curves was adjusted by a linear fit and subtracted in order to remove the paramagnetic contribution and calculate the hysteresis parameters ( $M_r$ ,  $M_s$ ,  $H_{cr}$  and  $H_c$ ). The coercivity of remanence ( $H_{cr}$ ) was also estimated during ‘back field’ IRM acquisition. The ratio of the hysteresis parameters ( $M_r/M_s$  versus  $H_{cr}/H_c$ ) was plotted on a Day diagram (Day *et al.* 1977).

Hysteresis loops characterize stable single-domain (SSD), pseudo-single-domain (PSD) and multidomain (MD) grain populations. A number of hysteresis loops are ‘wasp-waisted’ (dikes AB4 and AC1 in Suppl. file #1), which can result from combining two magnetic phases with differences in coercivity or from combining single domain and superparamagnetic (SP) grains (Tauxe *et al.* 1996). The ratio of the hysteresis parameters ( $M_r/M_s$  versus  $H_{cr}/H_c$ ) plotted in the Day diagram show that most of the samples

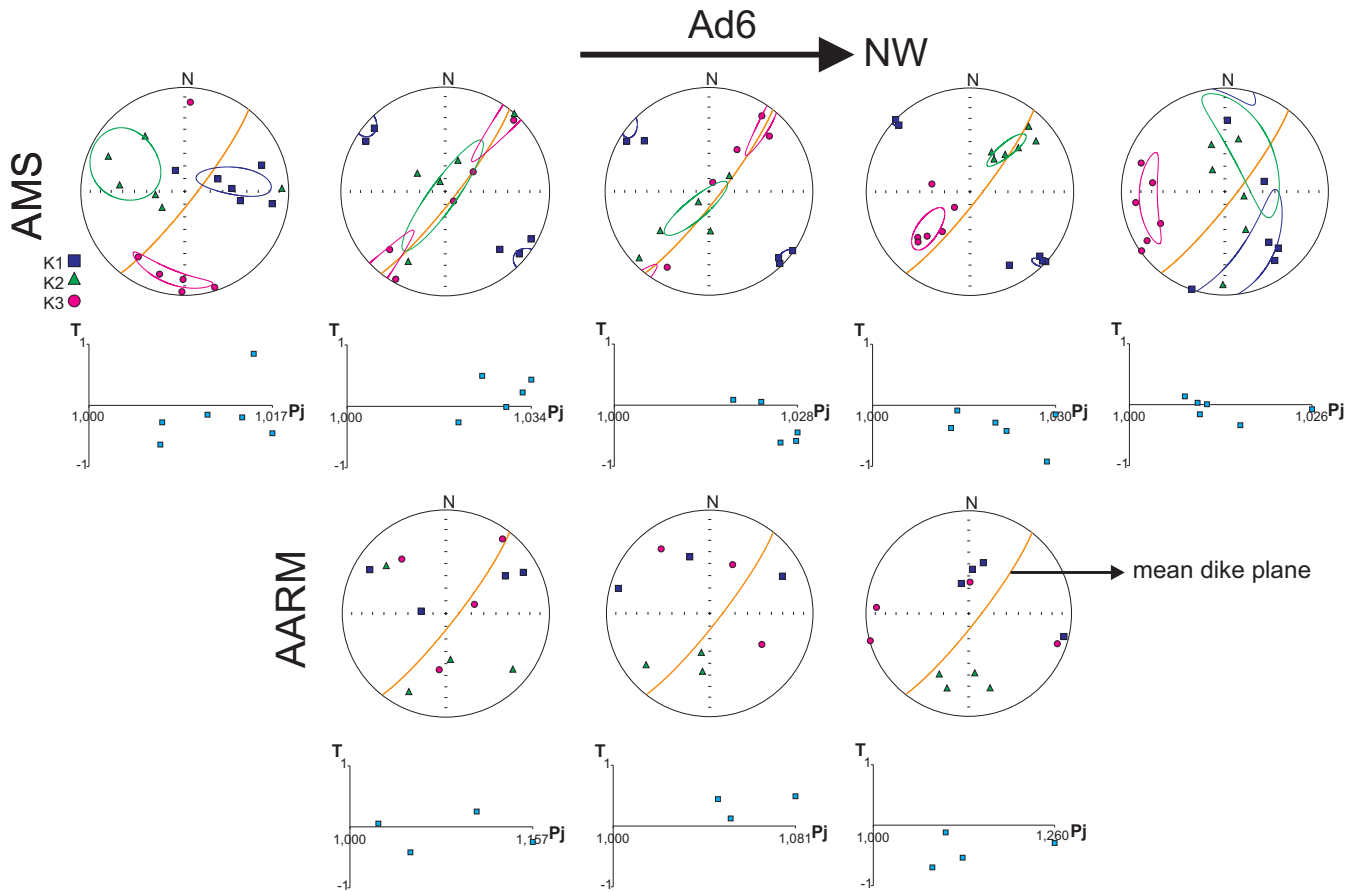


**Figure 8.** Equal-area lower-hemisphere stereograms of the principal AMS and AARM axes across profile of dike AD6. Diagrams of the corrected anisotropy degree ( $P'$ ) versus shape factor ( $T$ ) are shown for the AMS and the AARM.

fall in the PSD or SSD+MD region and in the SSD+SP region, as defined by Dunlop (2002) and Dunlop & Carter-Stiglitz (2006).

Samples from dike AD10, the only dike with a normal AMS fabric, fall in the PSD/SSD+MD region (Fig. 10), displaying the lowest  $M_r/M_s$  ratio and a trend that fits well with the predicted mixtures of SSD and MD end members (Dunlop & Carter-Stiglitz 2006). Overall, samples from the rest of dikes display a more sub-horizontal trend than AD10, indicating mixtures of different grain sizes and proportions of SSD and SP grains (Fig. 10). In particular, many samples fall in the region defined by Tauxe *et al.* (1996) for a log-normal distribution of SSD and SP grains with a SSD/SP threshold of 15 nm, although many samples also show trends that fit well with mixtures of SSD and SP grains as small as 8–10 nm (Dunlop & Carter-Stiglitz 2006). Samples from dike AC1 have the highest  $M_r/M_s$  ratio and the lowest  $H_{cr}/H_c$  ratio, plotting close to the SSD region (Fig. 10).

### 6.1 Diagrams of first order reversal curves (FORC's)

Most of the measured samples fall in the PSD/SSD+MD region and in the intersection area between this region and the SSD+SP region of the Day plot, leading to ambiguous domain-state characterization (Fig. 10). To clarify the domain-state characterization, we studied the hysteresis properties by measuring FORC's in selected samples across dike profiles (Figs 11–13).

The FORC diagram of a sample from the east margin of dike AD10 (normal fabric) shows outer contours diverging away from

the origin of the FORC diagram and extending along the  $H_u$  axis while inner contours are closed about a central peak at  $H_c = 70$  Oe (Fig. 11). This type of FORC distribution is characteristic of bimodal mixtures of SSD-MD grains, in which the central peak shifts towards higher coercivity values along the  $H_c$  axis and more contours are closed about this central peak as the SSD contribution in the magnetic signal increases (Roberts *et al.* 2000; Muxworthy *et al.* 2005; Carvallo *et al.* 2006; Kissel *et al.* 2010). Weak magnetostatic interactions can be inferred for dike AD10 based on the vertical spreading of contours along the  $H_u$  axis and on the width of the peak at  $H_u = 0$  in the vertical profile along  $H_c = 70$  Oe (Fig. 11). The FORC diagram of a sample from AD10 allows characterization of the domain state in this dike as a bimodal distribution of SSD-MD grains rather than a population of PSD grains.

FORC diagrams of samples from all dikes except AD10 have two peaks, which are also apparent in the horizontal profiles along  $H_u = 0$  (Figs 12 and 13). A peak is centered about the origin of the FORC diagram and another peak is centred at  $H_u = 0$  and at coercivities ranging from 70 Oe to 500 Oe. In these FORC diagrams, the peak about the origin is shifted towards  $H_u > 0$  while the peak at high coercivity is shifted towards  $H_u < 0$ . As a result, the two peaks are not aligned along  $H_u = 0$  and the overall contours of the FORC distribution appear slightly tilted clockwise with respect to the origin (Figs 12 and 13). Most of these FORC diagrams have steep, nearly vertical, outer contours in the lower half of the FORC distribution and inner contours of the peak about the origin intersecting the  $H_u$  axis. Shifting of the peaks above and below  $H_u = 0$  has been also observed in those FORC distributions having just one peak, whether

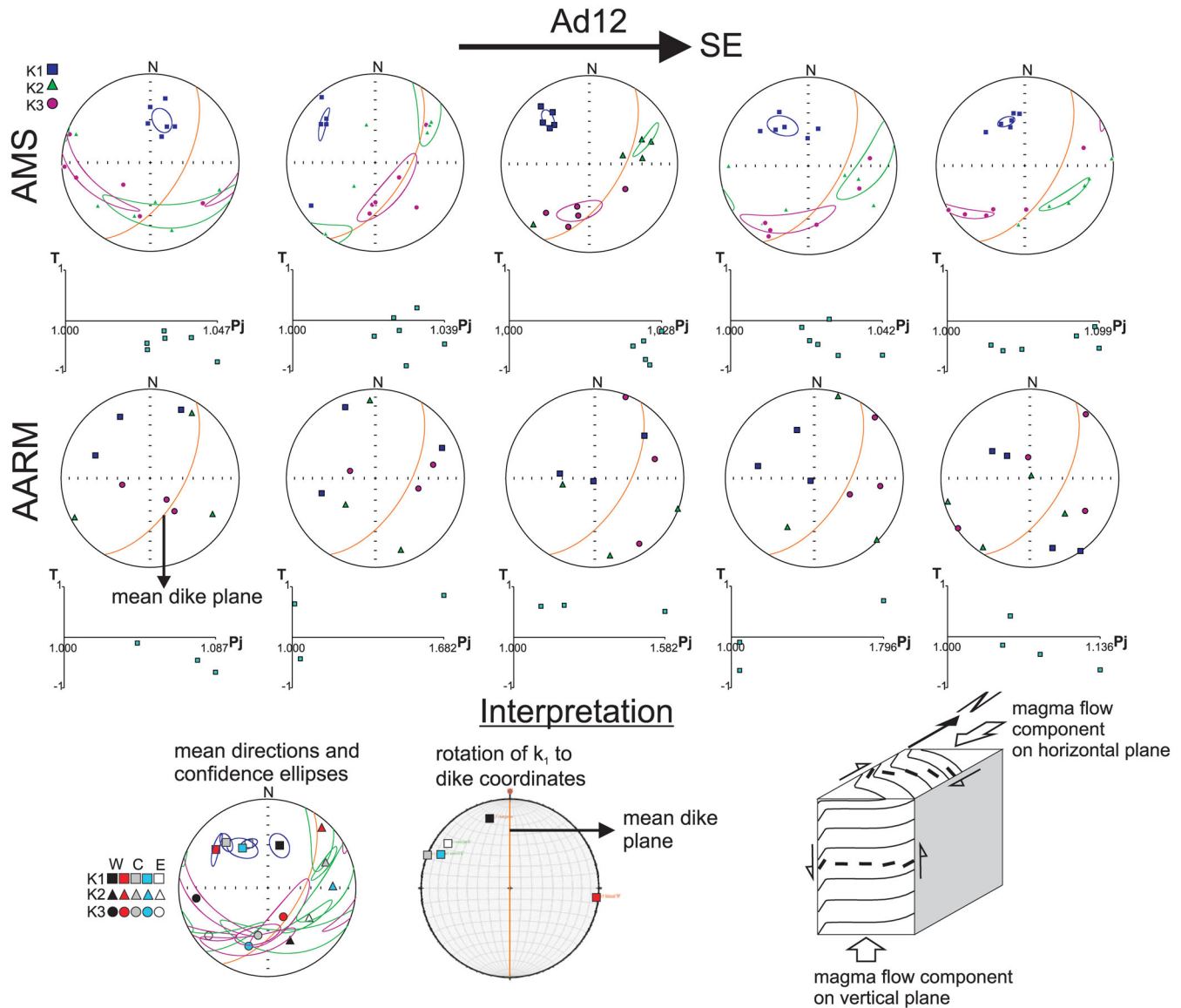


**Figure 9.** Equal-area lower-hemisphere stereograms of the principal AMS and AARM axes across profile of dike AD12. Diagrams of the corrected anisotropy degree ( $P_j$ ) versus shape factor ( $T_j$ ) are shown for the AMS and the AARM. Interpretation of the fabric AMS asymmetry in terms of magma flow and remote shear resolved on the dike plane is done after rotation of the mean directions of  $K_1$  axes to the dike coordinates (see text for discussion).

it is about the origin (AB4-7b in Fig. 12) or at high coercivity (AC1-34a and AC1-12b in Fig. 12).

FORC diagrams with two peaks at  $H_u = 0$  are characteristic of SSD-SP mixtures, in which the peak about the origin corresponds to the SP grains and the peak at higher coercivity corresponds to the SSD grains (Roberts *et al.* 2000; Pike *et al.* 2001). Steep, nearly vertical, outer contours in the lower half of the FORC distribution indicates the presence of SP grains, whereas inner contours of the peak at the origin intersecting the  $H_u$  axis has been interpreted as due to thermal relaxation effects (Roberts *et al.* 2000; Pike *et al.* 2001). Shifting of the peak at high coercivity below  $H_u = 0$  is attributed to the effects of magnetostatic interactions, whereas shifting of the peak about the origin above  $H_u = 0$  is attributed to thermal relaxation effects (Roberts *et al.* 2000; Pike *et al.* 2001; Muxworthy *et al.* 2004). Hence, clockwise tilting of the FORC distribution is due to the competition between interaction and thermal relaxation effects (Pike *et al.* 2001). In particular, dike AD12 has a two-peak FORC distribution in which the SP peak is above  $H_u = 0$  and

the SSD peak is below  $H_u = 0$  and magnetostatic interactions are expected in this dike from the closely spaced distribution of Fe-Ti oxides along chains subparallel to  $K_1$  (Fig. 2F). Overall, FORC diagrams of dikes with anomalous fabrics can be attributed to bimodal mixtures of SSD-SP grains.

## 6.2 Distribution of SSD and SP grains inferred from FORC diagrams

Horizontal profiles of FORC diagrams with mixtures of SSD-SP grains suggest that the bimodal distribution of SSD and SP grains is overlapped (Figs 12 and 13). FORC diagrams of two specimens drilled within a distance of less than 10 cm from each other on the east margin of dike AD12 show two peaks (AD12-5 in Fig. 13) and just a peak about the origin (not shown), suggesting that the bimodal distribution of SSD and SP grains is overlapped at the scale of the group of cores on this margin. In addition, FORC diagrams of two

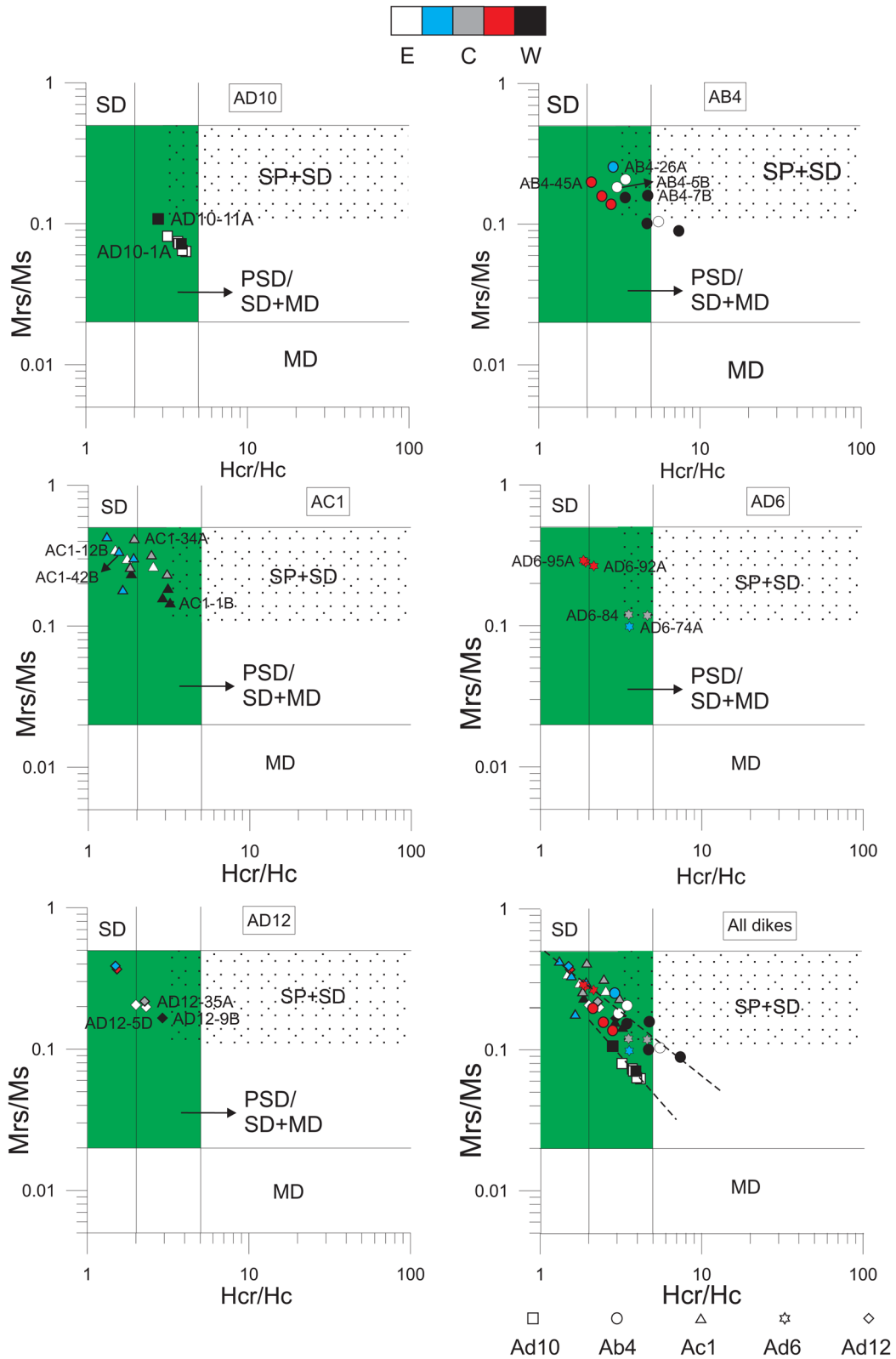


**Figure 10.** Day plots of the hysteresis parameters ( $M_r/M_s$  versus  $H_{cr}/H_c$ ) of samples across dike profiles for each particular dike and for all dikes. The colour code indicates the position of samples across dike profiles. The approximate trends for dike AD10 and for the rest of the dikes are shown.

specimens drilled within a distance of less than 50 cm in the group of cores of the intermediate position between the centre and the west margin of dike AD6 have two peaks, and the high coercivity peak varies in intensity and coercivity from one sample to the other

(Fig. 13). This feature confirms that the bimodal distribution of SSD and SP grains is also overlapped at the scale of this group of cores in AD6. As shown by Pike *et al.* (2001) for normal-resolution FORC's of SSD and SP samples, a secondary peak would have been

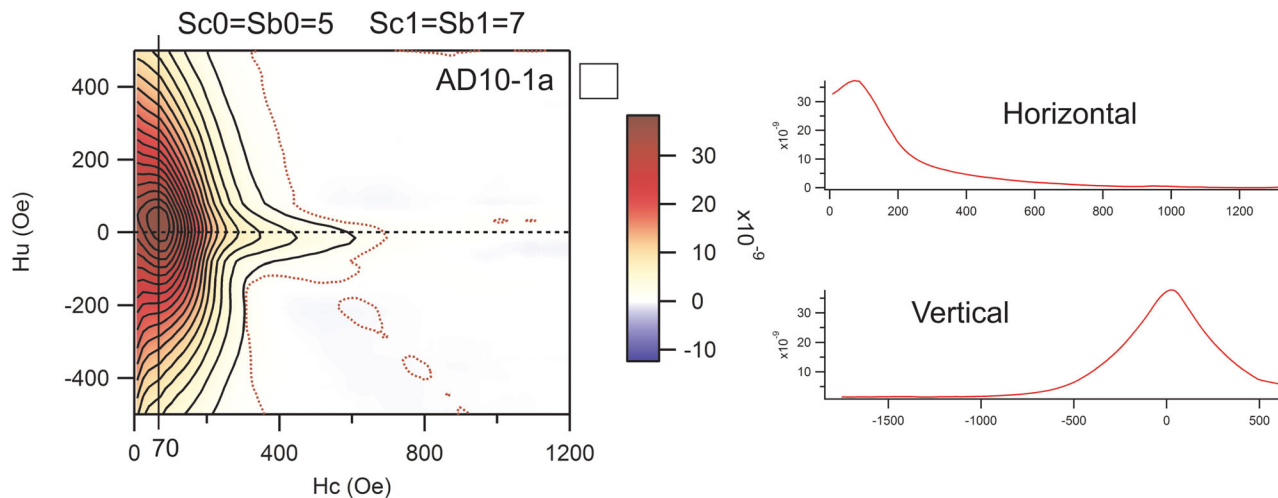


**Figure 11.** FORC diagram and profiles of the FORC distribution of a sample from dike AD10. Horizontal profile is performed along  $H_u = 0$  and vertical profile is located in the FORC diagram. See colour code in Fig. 10 to locate the sample across dike profile.

probably enhanced by high-resolution FORC experiments in those diagrams with just one peak (AB4-7b, AC1-34a and AC1-12b in Fig. 12). Nevertheless, the differences of normal-resolution FORC diagrams across dike profiles arise from the intensity and coercivity of one of the two peaks and from the lack of one peak. These differences allow for a qualitative assessment on the contribution of SSD and SP grains in the bimodal distributions across dike profile. Hence, SSD grains would be dominant in the centre and east margin of dike AC1, whereas SP grains would dominate the bimodal mixture on the west margin of dike AB4 (Fig. 12). The grain size window upon which SSD and SP grains are overlapped depends on the particle anisotropy and on the degree of Ti substitution in the titanomagnetite lattice (Butler & Banerjee 1975; Tauxe *et al.* 1996; Dunlop & Carter-Stiglitz 2006). Based on the SSD-SP threshold estimations in previous studies and on the degree of Ti substitution observed in the studied dikes (Fig. 4), the grain size window upon which SSD and SP grains are overlapped can be conservatively approximated at 10–50 nm (Butler & Banerjee 1975; Tauxe *et al.* 1996; Dunlop & Carter-Stiglitz 2006).

## 7 DISCUSSION

The origin of inverse AMS fabrics has been the subject of some debate. The explanations currently given for inverse fabrics can be grouped into three types.

(1) Inverse AMS caused by the cyclic rotation of magnetic particles. Ellipsoidal particles in a viscous fluid undergo cyclic rotation around the shear plane within the flow (Jeffery 1922). Inverse AMS fabrics would result from particles oriented perpendicular to the shear plane when the flow froze (Dragoni *et al.* 1997; Cañón-Tapia & Chávez-Álvarez 2004).

(2) Inverse AMS is caused by elongated SSD magnetite. Elongated SSD magnetite has zero susceptibility parallel to the long axis of the particle and maximum susceptibility perpendicular to it (Potter & Stephenson 1988). In rocks dominated by elongated SSD magnetite, it is assumed that the long axes of SSD magnetites are parallel to the flow and to the dike plane. Hence, the measured AMS will show  $K_1$  axes perpendicular to long axes of SSD magnetites and to the dike plane. Inverse AMS fabrics due to SSD particles can be identified by the anisotropy of magnetic remanence (for example AARM). Elongated SSD magnetite has maximum remanence par-

allel to the long axis of the particle. Therefore, rocks dominated by elongated SSD magnetite will show  $K_1$  axes of the AARM perpendicular to  $K_1$  axes of the AMS (Potter & Stephenson 1988; Rochette *et al.* 1991).

(3) Other causes of inverse AMS fabrics include a number of syn- to post-magma emplacement processes, such as late-stage crystallization of magnetic phases, alteration, post-emplacement crystallization and tectonic stresses. These processes may yield superimposed fabrics to the flow-related fabric, which is assumed to be parallel to the dike plane (Walderhaugh 1993; Tauxe *et al.* 1998; Rochette, *et al.* 1999; Raposo and D'Agrella-Filho 2000; Féménias *et al.* 2004). Some superimposed fabrics occur during late stages of magma cooling perpendicular to the external cooling surface of the magma body (Moore & Lockwood, 1973).

From a geometric point of view, ellipsoidal particles undergoing cyclic rotation in a viscous fluid may orient at any angle with respect to the shear plane of the flow when the flow freezes (Dragoni *et al.* 1997; Cañón-Tapia & Chávez-Álvarez 2004). However, experimental and empirical data show that, due to fluid viscosity and particle interactions, particles tend to align parallel to the shear plane of the flow and to imbricate at low angles with respect to it (Ildefonse *et al.* 1992; Nicolas 1992; Arbaret *et al.* 1996). Oriented thin sections of the studied dikes have some microlites and small crystals in the groundmass at high angles ( $>60^\circ$ ) with respect to the dominant silicate fabric, in particular when the groundmass wraps around corners of larger phenocrysts. Nevertheless, the statistical significance of these high-angle particles can be neglected with respect to the dominant fabric at the thin-section scale because most microlites and small crystals are parallel to the silicate fabric or imbricate at an angle of less than  $30^\circ$  (Fig. 2). Inverse AMS fabrics of the studied dikes are generally well grouped and correspond to groups of six specimens drilled within a short distance ( $<50$  cm) of each other (Figs 1 and 6–9). This means that inverse AMS fabrics are statistically significant at the scale of each group of cores. The AMS of the studied dikes is mainly carried by titanomagnetite and the silicate fabric is assumed to be flow related. Given the statistical significance of inverse AMS fabrics and that they are perpendicular to silicate fabrics, it seems unlikely that inverse AMS fabrics of the studied dikes are caused by the cyclic rotation of titanomagnetite grains oriented at high angles to the shear plane of the flow when the magma froze.

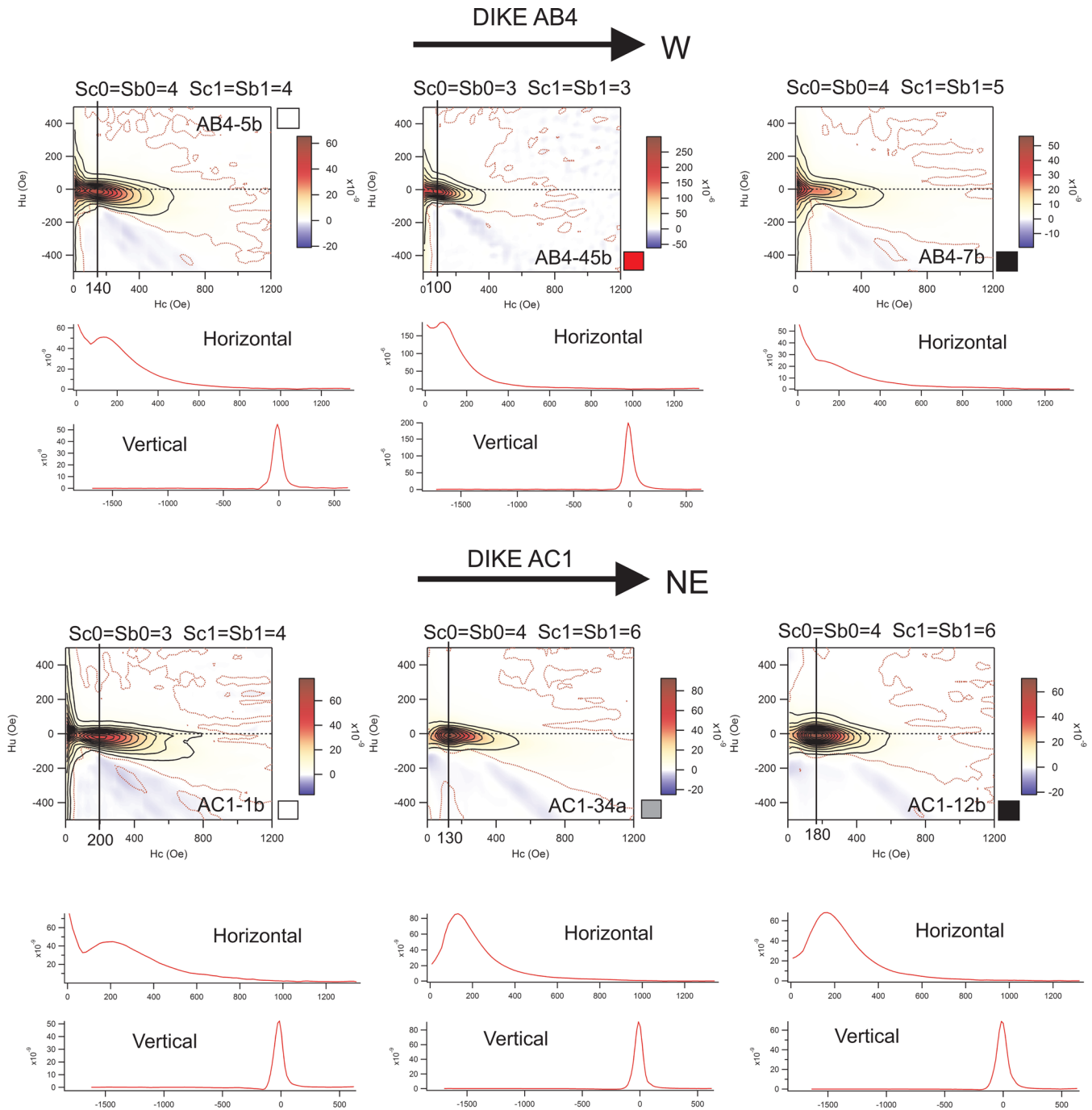


**Figure 12.** FORC diagrams and profiles of the FORC distributions of samples from dikes AB4 and AC1. Horizontal profile are performed along  $H_u = 0$  and vertical profiles are located in the FORC diagram. See colour code in Fig. 10 to locate samples across dike profile.

### 7.1 Domain state controls on inverse AMS fabrics and AARM fabrics

The stability of magnetic particles in the SSD-SP threshold is properly described in the Néel theory, which predicts the stability of SSD particles as a function of thermal activation and particle volume and that there is a characteristic relaxation time below which SSD particles are unstable and become superparamagnetic (Néel 1949). For a given volume, the relaxation time strongly depends on the shape anisotropy of the particle (Butler & Banerjee 1975). For example, ellipsoidal magnetite of 15 nm width relaxes in  $10^{-3}$  s whereas ellipsoidal magnetite of 20 nm width relaxes in 11 d (Tauxe 2010).

Magnetic susceptibility of SSD particles is limited by the shape anisotropy, whereas the susceptibility of SP particles involves complete rotation of the particles' magnetic moments (Worm & Jackson 1999). As a result, mixtures of SSD and SP grains dominated by SP particles will have much higher susceptibility than SSD-dominated mixtures. Conversely, SSD particles are stable carriers of magnetic remanence and have much higher susceptibility of the ARM than SP particles. Empirical data on magnetite in the SSD-SP threshold of the Tiva Canyon Tuff show a decrease in the magnetic susceptibility and an increase in the susceptibility of the ARM as the domain state changes up section from SP-dominated to stable SD mixtures

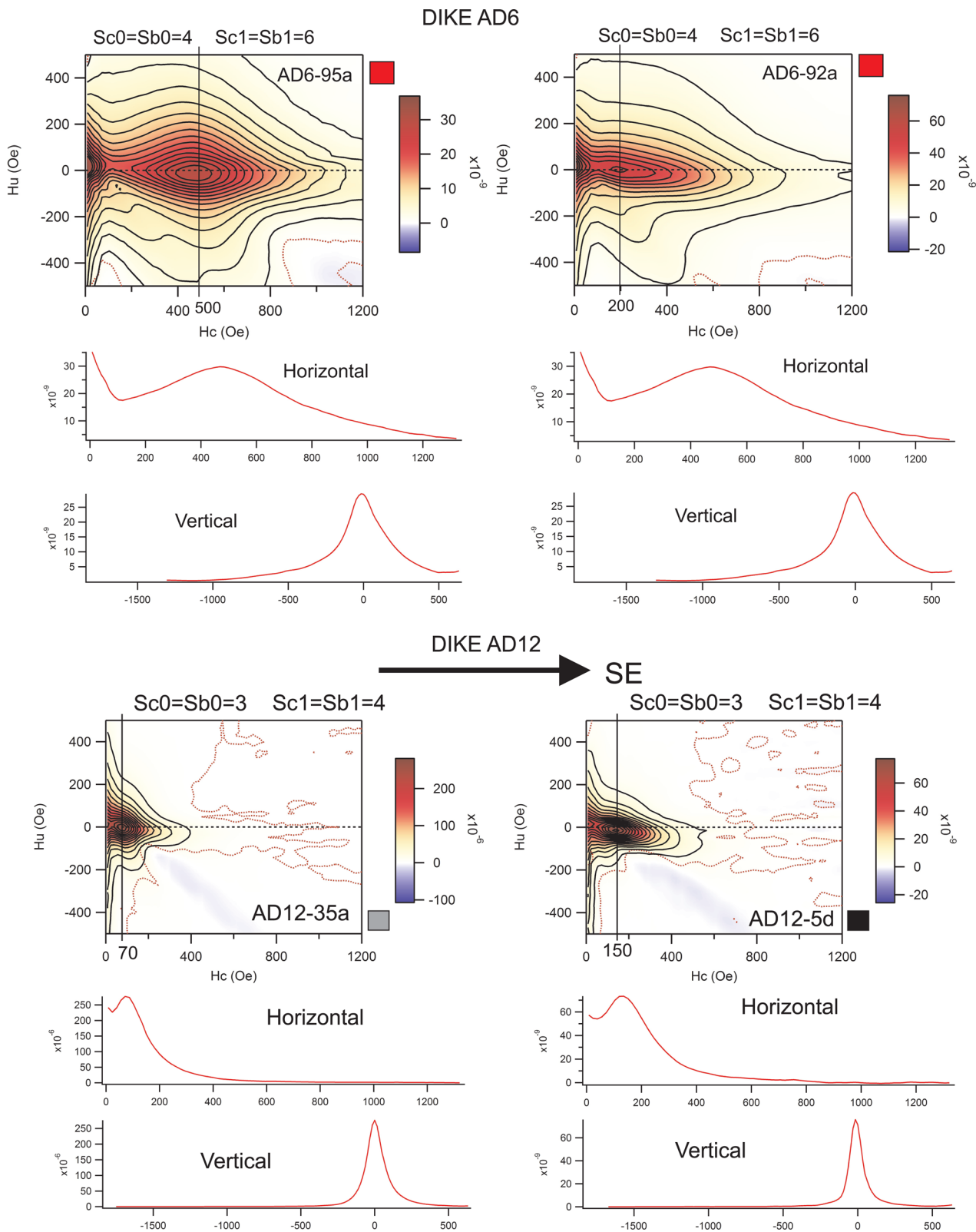


**Figure 13.** FORC diagrams and profiles of the FORC distributions of samples from dikes AD6 and AD12. Horizontal profile are performed along  $H_u = 0$  and vertical profiles are located in the FORC diagram. See colour code in Fig. 10 to locate samples across dike profile.

(Till *et al.* 2011). Magnetostatic interactions are also known to have some effects in the ARM and in the stability of magnetic particles in the SSD-SP threshold (Egli 2006; Muxworthy & Williams 2009). The remanence of some ellipsoidal magnetites within the SSD-SP

threshold (for example within the 15–20 nm range at a given shape anisotropy) will be measured in conventional AARM experiments, displaying maximum susceptibility of the AARM along the long axis while these particles will likely have maximum susceptibility

of the AMS along their long axis too. The resultant AMS and AARM fabrics of samples dominated by this grain size range will be coaxial and parallel. Overall, the larger the contribution of SP grains in the bimodal mixture of SSD-SP, the more aligned the AMS and AARM fabrics will be. Recently, Hrouda & Ježek (2014) have shown that in the SSD-SP transition not only the susceptibility depends on the frequency of the applied field but also the AMS fabric is frequency-dependent. By measuring the AMS at different frequencies and subtracting the corresponding signal one might be able to estimate the contribution of SSD and SP grains sizes. It is a promising method still under development that is on the edge of the accuracy possibilities of the most sensitive instruments available (Hrouda & Ježek 2014).

Hysteresis loops, hysteresis parameters and FORC diagrams of the studied dikes indicate that dikes with inverse AMS fabrics are dominated by bimodal mixtures of SSD and SP particles with an overlapped distribution of SSD and SP grains. However, some of the AARM fabrics across dike profiles do not have  $K_1$  axes of the AARM perpendicular to  $K_1$  axes of the AMS, as would be expected for dikes in which there is a significant contribution of elongated SSD magnetite (Potter & Stephenson 1988).

Dike AC1 has an inverse AMS fabric in the east margin and the FORC diagram of sample AD1-12b suggests that SSD grains dominate the bimodal mixture of SSD and SP grains (Fig. 14). The  $K_1$  axes of the AARM in this margin are distributed along the dike plane and are perpendicular to  $K_1$  axes AMS. This is in good agreement with inverse AMS caused by elongated SSD magnetite as predicted by Potter & Stephenson (1988).

However, dike AC1 has an inverse AMS fabric in the west margin but  $K_1$  axes of the AARM are neither perpendicular nor parallel to  $K_1$  axes of the AMS but at about an angle of  $45^\circ$ . The FORC diagram of sample AC1-1b in this margin is characteristic of a bimodal mixture of SSD and SP grains (Fig. 14). Dike AB4 has an inverse AMS fabric in the east margin and a coaxial (parallel) AARM fabric while the FORC diagram of AB4-5b is characteristic of a bimodal mixture of SSD and SP (Fig. 15). Hence, it does not indicate an inverse AMS fabric caused by elongated SSD magnetite. In the west margin of AB4,  $K_1$  axes of the AARM are somewhat dispersed and closer to the dike plane than  $K_1$  axes of the inverse AMS fabric but the AARM  $K_1$  axes are not perpendicular to the AMS  $K_1$  axes as would be expected for inverse AMS caused by elongated SSD magnetite (Fig. 15). Besides, in this margin the FORC diagram of AB4-7b suggests that SP grains dominate the bimodal mixture of SSD and SP grains (Fig. 15). Dike AD6 has an inverse AMS fabric in the group of samples between the west margin and the dike centre and  $K_1$  axes of the AARM are at about  $50^\circ$  to  $K_1$  axes of the AMS, whereas the FORC diagrams of two samples from this group of cores are characteristic of a bimodal mixture of SSD and SP grains (Figs 8 and 13).

The former examples showing non-perpendicular AMS and AARM fabrics suggest that interpretation of inverse AMS fabrics and AARM fabrics of bimodal mixtures of SSD and SP grains with overlapped distributions can be complex and that the causes of inverse AMS fabrics cannot be explained solely by the contribution of elongated SSD magnetite.

## 7.2 Interpretation of inverse AMS fabrics and AARM fabrics

Dikes AB4 and AC1 illustrate the different combinations of silicate fabrics, inverse AMS fabrics, AARM fabrics and FORC diagrams

observed in the studied dikes. In our discussion, we assume uniaxial anisotropy of ferromagnetic grains and use these two dikes as case studies for the interpretation of dike petrofabrics (Figs 14 and 15).

The secondary peak in FORC distributions of dike AC1 is usually at higher coercivity than the secondary peak in FORC distributions of dike AB4 (Fig. 12). In addition, dike AC1 has two FORC distributions with just one peak at high coercivity (east margin and dike centre) while AB4 has a FORC distribution with just a peak about the origin (west margin). Hence, SD titanomagnetites seem to be larger and more stable in dike AC1 than in AB4.

The FORC diagram of a sample from the west margin of dike AC1 indicates a mixture of SSD-SP grains with a bimodal distribution (Fig. 14). The silicate fabric is parallel to the dike plane whereas  $K_1$  axes of the AARM are at about  $45^\circ$  to  $K_1$  axes of the inverse AMS fabrics. In the west margin of AC1, the AMS and AARM are likely dominated by SD titanomagnetite grains subparallel to the silicate fabric and to the dike plane (Fig. 14). In the dike centre, the  $K_1$  axes of the AMS fabric are distributed on two clusters, one cluster on the dike plane and the other perpendicular to it. This two-cluster distribution yields large confidence ellipses and confidence angles and difficult the interpretation of AMS fabric so we have focused on the interpretation of the sample measured in FORC experiments. The FORC distribution of AC1-34a is characteristic of SSD-SP mixtures in which SSD is dominant. The peak of the FORC distribution has the lowest coercivity value of dike AC1, which can be interpreted as finer grain size in the dike centre (Fig. 12). AMS and AARM fabrics for this sample are coaxial (parallel), which would not be expected in a sample with dominant SSD grains. A possible interpretation is that a significant proportion SD titanomagnetites in sample AC1-34a correspond to equant grains with cubic anisotropy rather than elongated grains with uniaxial anisotropy, which could result in the AMS dominated by the paramagnetic and SP fractions. In the east margin of AC1,  $K_1$  axes of the AARM are perpendicular to  $K_1$  axes of the inverse AMS fabric and are parallel to the silicate fabric and to the dike plane. Here, the AMS and AARM are inferred to be dominated by SSD titanomagnetite grains oriented parallel to the dike plane (Fig. 14). Overall, the petrofabrics of dike AC1 can be characterized as flow related.

The FORC diagram of a sample from the east margin of dike AB4 indicates a mixture of SSD-SP grains with a bimodal distribution. The silicate fabric is parallel to the dike plane whereas the AMS and AARM fabrics are coaxial (parallel) and perpendicular to the dike plane (Fig. 15). These features suggest that the AMS fabric is controlled by SP grains oriented perpendicular to the dike plane that probably crystallized against the dike wall during magma cooling after the shear flow of magma had stopped. The FORC diagram of a sample from the west margin of dike AB4 indicates a mixture of SSD-SP grains with a bimodal distribution dominated by SP grains (Fig. 15). In the west margin of AB4, the silicate fabric is parallel to the dike plane and  $K_1$  axes of the AARM are disperse and closer to the dike plane than  $K_1$  axes of the inverse AMS fabric. Here, the AMS would be controlled by SP grains perpendicular to the dike plane while the AARM would be controlled by SSD grains of the mixture oriented in the same way. This is a likely interpretation considering the large susceptibility and degree of AMS of SP grains (Worm & Jackson 1999; Hrouda & Ježek 2014). In the intermediate positions between the dike centre and both margins, the FORC diagram indicates a mixture of SSD-SP grains with a bimodal distribution, whereas AMS and AARM fabrics are coaxial (parallel) and parallel to the dike plane and to the silicate fabric (Fig. 15). Here, the AMS fabric would be controlled by SP grains oriented parallel

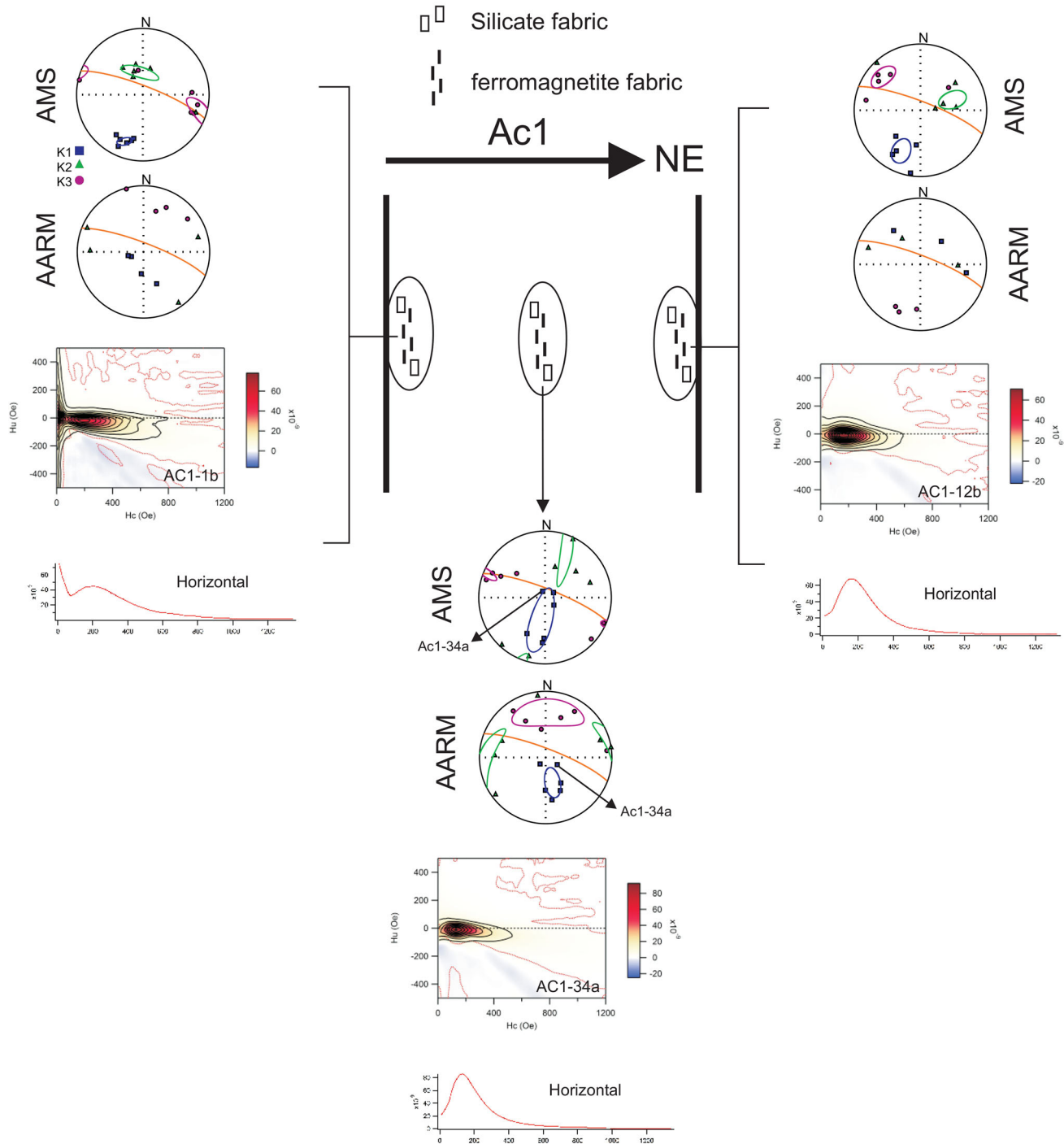


**Figure 14.** Interpretation of the petrofabrics of dike AC1 based on AMS and AARM fabrics and on FORC distributions (see text).

to the dike plane and the AARM fabric would be dominated by SSD grains of the bimodal mixtures. Overall, the petrofabrics of AB4 can be characterized as flow related except on both margins, where crystallization of ferromagnetic minerals during cooling took place against the dike wall once the viscous flow of magma had stopped. The orientation of these magnetic crystals may be related to nucleation and crystal growth dynamics, if nucleation was near the cooling surface and growth was perpendicular to that. Such crystal growth patterns are seen in some dikes elsewhere (e.g. Moore & Lockwood, 1973).

In rocks with bimodal mixtures of titanomagnetite in the SSD-SP threshold,  $K_1$  axes of the AMS are expected to be coaxial (parallel) with  $K_1$  axes of the AARM when SP grains are dominant. Conversely,  $K_1$  axes of the AMS are expected to be coaxial (perpendicular) with  $K_1$  axes of the AARM when SSD grains dominate the bimodal mixture. However, angular differences of 45–50° between  $K_1$  axes of the AMS and  $K_1$  axes of the AARM has been observed in some groups of samples and individual samples of the studied dikes (e.g. west margin of AC1, west margin of AB4, centre and intermediate positions of AD6). These angular differences are difficult to

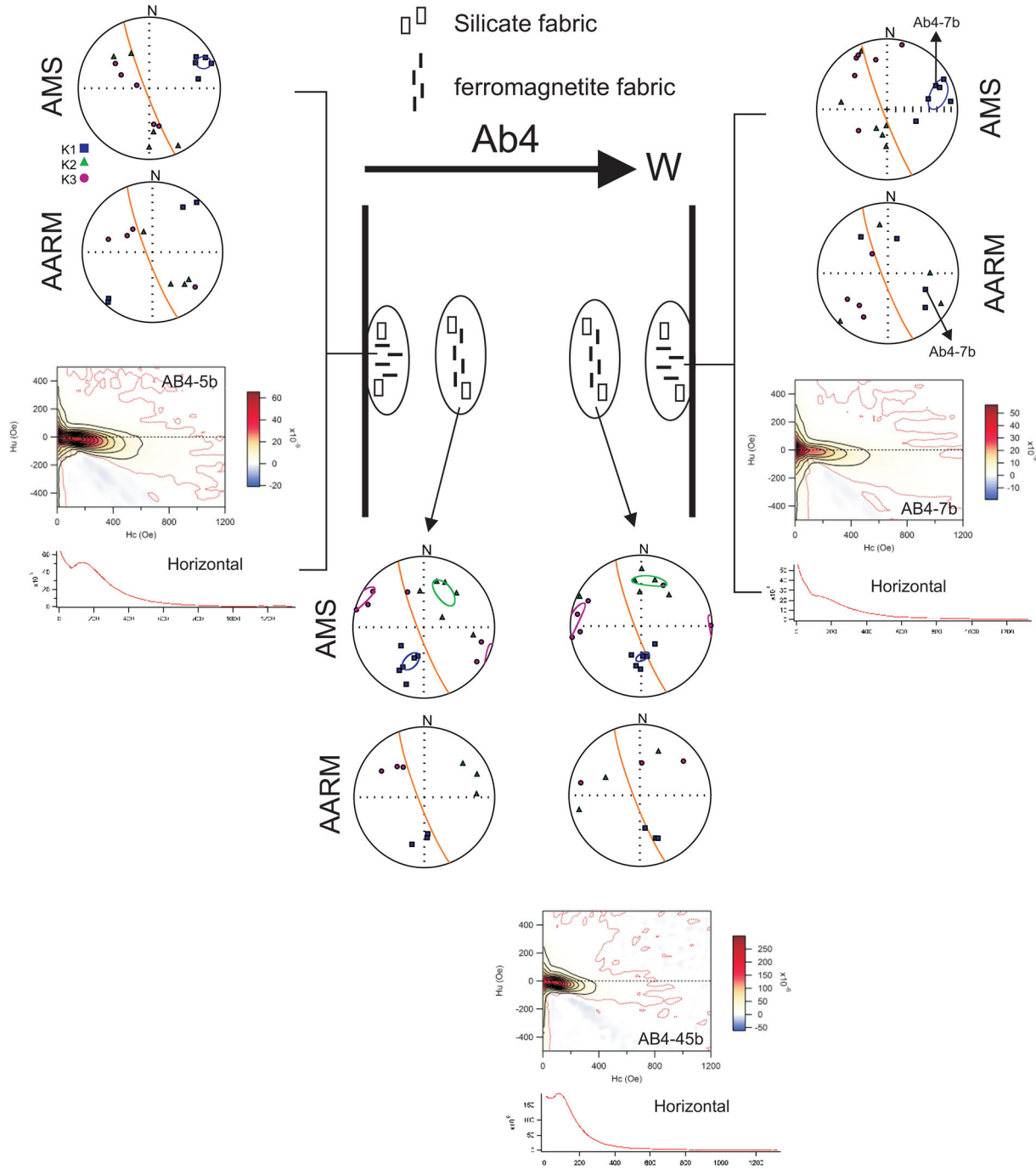


Figure 15. Interpretation of the petrofabrics of dike AB4 based on AMS and AARM fabrics and on FORC distributions (see text).

explain in terms of stability of SD grains and grain size predominance in the bimodal mixtures of SSD and SP grains. Although in rocks with high bulk susceptibilities ( $>1 \times 10^{-3}$  SI) like the dikes studied here the AMS is inferred to be dominated by ferromagnetic minerals (Rochette *et al.* 1991; Hrouda 2002), we suggest that the paramagnetic fraction has played a significant role in the orientation AMS axes and can explain the angular differences observed. In particular, skeletal and acicular ulvospinel grains, which are abundant in the studied dikes and frequently non-parallel to the silicate and ferromagnetic fabrics, may have contributed to the observed non-coaxiality between AMS and AARM fabrics (Fig. 2). Equant SSD titanomagnetites with cubic anisotropy may have also enhanced the

paramagnetic and SP contributions in the AMS while having bulk susceptibilities typical of ferromagnetic minerals.

## 8 CONCLUSIONS

The study of AMS data in dikes allows characterization of magma flow as derived from the orientation of magnetic fabrics. Magnetic foliation parallel or imbricated at low angles against the dike wall is referred to as normal fabric, and allows straightforward interpretation of magma flow. Unfortunately, AMS analysis often yields anomalous results in which the orientation of the magnetic ellipsoid does not meet the basic requirements for magma flow

interpretations. A particular type of these anomalous fabrics is the case of magnetic foliation perpendicular to dike walls, generally referred to as inverse fabric.

A known source of anomalous fabrics is the peculiar behaviour of elongated, very fine-grained SSD magnetite. These particles have their maximum susceptibility axes oriented at right angles with respect to particle elongation, so that the AMS ellipsoid does not represent the rock fabric. Decoding the contribution of SSD magnetite to AMS fabrics can be assessed by comparison with the remanence anisotropy obtained by means of the AARM data. We document cases of both parallel and perpendicular AMS and AARM ellipsoids for dikes from rift zones of the Miocene basaltic shield of Tenerife, Canary Islands. Cases of AARM ellipsoids perpendicular to AMS ellipsoids clearly indicate the presence of elongated SSD magnetite particles. Here, magma flow can only be inferred from the orientation of the AARM ellipsoid. AARM ellipsoids that parallel the AMS ellipsoids indicate that the magnetic fabric coincides with the particle fabric. In such cases, an inverse magnetic fabric may represent post-emplacement *in situ* crystal growth perpendicular to dike walls, and therefore unrelated to magma flow.

In dikes dominated by magnetic particles at the SSD-SP threshold, FORC experiments are a useful method to investigate the relative abundance of SP particles in bimodal mixtures of SSD and SP grains and the effects on AMS and AARM fabrics. We suggest that SP particles near the SSD-SP threshold may experience relaxation times sufficient to retain the magnetic remanence at the time scale of the laboratory experiments. This fraction of SP particles would contribute to both the AMS and the AARM data with coaxial distributions of their anisotropy axes, so that the larger the SP fraction is in the mixture, the greater the similarity will be between the AMS and AARM fabrics. We also document some cases in which AMS and AARM ellipsoids are non-coaxial and their respective axes show angular relations of about 45°. These cases cannot be explained by the relative abundance of SP grains in bimodal mixtures and it is suggested that paramagnetic ulvospinel minerals non-parallel to the ferromagnetic and silicate fabrics may be responsible for the observed angular relation between AMS and AARM ellipsoids.

The combination of a number of magnetic experiments like AMS, AARM and FORC's may help to understand those magnetic fabrics currently typified as anomalous and discarded for AMS studies in terms of magma flow, magma emplacement and magma cooling processes.

## ACKNOWLEDGEMENTS

We thank Roberto Lanza for his warm welcome at the Alpine Laboratory of Palaeomagnetism (ALP) in Italy. We also thank Claudia Álvarez for conducting some of the FORC measurements at the CE-NIEH. This research has been partly funded by project CGL2008-04264/BTE and by grant PRX14/00303 to Carles Soriano.

## REFERENCES

- Arbaret, L., Diot, H. & Bouchez, J.-L., 1996. Shape fabrics of particles in low concentration suspensions: 2D analogue experiments and application to tilting in magma, *J. Struct. Geol.*, **18**, 941–950.
- Aubourg, C., Giordano, G., Mattei, M. & Speranza, F., 2002. Magma flow in sub-aqueous rhyolitic dikes inferred from magnetic fabric analysis (Ponza Island, W. Italy), *Phys. Chem. Earth*, **27**, 1263–1272.
- Borradaile, G.J. & Gauthier, D., 2003. Interpreting anomalous magnetic fabrics in ophiolite dikes, *J. Struct. Geol.*, **25**, 171–182.
- Butler, R.F. & Banerjee, S.K., 1975. Theoretical single domain grain-size range in magnetite and titanomagnetite, *J. geophys. Res.*, **80**, 4049–4058.
- Callot, J.P. & Guichet, X., 2003. Rock texture and magnetic lineation in dykes: a simple analytical model, *Tectonophysics*, **366**, 207–222.
- Callot, J.-P., Geoffroy, L., Aubourg, C., Pozzi, J.P. & Mege, D., 2001. Magma flow directions of shallow dikes from the East Greenland volcanic margin inferred from magnetic fabric studies, *Tectonophysics*, **335**(3–4), 313–329.
- Cañón-Tapia, E., 1996. Single-grain versus distribution anisotropy: a simple three-dimensional model, *Phys. Earth planet. Inter.*, **94**, 149–158.
- Cañón-Tapia, E. & Chávez-Álvarez, M.J., 2004. Theoretical aspects of particle movement in flowing magma: implications for the anisotropy of magnetic susceptibility of dykes, in *Magnetic Fabric: Methods and Applications*, Vol. **238**, pp. 227–249, eds Martin-Hernández, F. et al. Geological Society Special Publication, The Geological Society of London.
- Carvalho, C., Muxworthy, A.R. & Dunlop, D.J., 2006. First-order reversal curve (FORC) diagrams of magnetic mixtures: micromagnetic models and measurements, *Phys. Earth planet. Inter.*, **154**, 308–322.
- Chadima, M., Cajz, V. & Týcová, P., 2009. On the interpretation of normal and inverse magnetic fabric in dikes. Examples from the Eger Graben, NW Bohemian Massif, *Tectonophysics*, **466**, 47–63.
- Correa-Gomes, L.C., Souza Filho, C.R., Martins, C.J.F.N. & Oliveira, E.P., 2001. Development of symmetrical and asymmetrical fabrics in sheet-like igneous bodies: the role of magma flow and wall-rock displacements in theoretical and natural cases, *J. Struct. Geol.*, **23**, 1415–1428.
- Cox, A. & Doell, R.R., 1967. Measurement of high-coercivity magnetic anisotropy, in *Methods in Paleomagnetism*, pp. 477–482, eds Collinson, D.W., Creer, K.M. & Runcorn, S.K., Elsevier.
- Day, R., Fuller, M. & Schmidt, V.A., 1977. Hysteresis properties of titanomagnetites: grain size and composition dependence, *Phys. Earth planet. Inter.*, **13**, 260–267.
- Delcamp, A., Petronis, M.S. & Troll, V.R., 2014. Discerning magmatic flow patterns in shallow-level basaltic dykes from the NE rift zone of Tenerife, Spain, using the Anisotropy of Magnetic Susceptibility (AMS) technique, in *The Use of Palaeomagnetism and Rock Magnetism to Understand Volcanic Processes*, Vol. **396**, pp. 87–106, eds Ort, M. H., Porreca, M. & Geissman, J.W., Geological Society Special Publications, The Geological Society of London.
- Dragoni, M., Lanza, R. & Tallarico, A., 1997. Magnetic anisotropy produced by magma flow: theoretical and experimental data from Ferrar dolerite sills (Antarctica), *Geophys. J. Int.*, **128**, 230–240.
- Dunlop, D.J. 2002. Theory and application of the Day plot (Mrs/Ms versus Hcr/Hc): theoretical curves and tests using titanomagnetite data, *J. geophys. Res.*, **107**, 2056.
- Dunlop, D.J. & Carter-Stiglitz, B., 2006. Day plots of mixtures of superparamagnetic, single-domain, pseudosingle-domain, and multidomain magnetites, *J. geophys. Res.*, **111**, B12S09.
- Egli, R., 2006. Theoretical considerations on the anhysteretic remanent magnetization of interacting particles with uniaxial anisotropy, *J. geophys. Res.*, **111**, B12S18.
- Egli, R., 2013. VARIFORC: an optimized protocol for the calculation of non-regular first-order reversal curve (FORC) diagrams, *Global planet. Change*, **110**, 302–320.
- Ellwood, B.B., 1978. Flow emplacement direction determined for selected basaltic bodies using magnetic susceptibility anisotropy measurements, *Earth planet. Sci. Lett.*, **41**, 254–264.
- Eriksson, P.I., Riishuus, M.S. & Elming, Å., 2014. Magma flow and palaeostress deduced from magnetic fabric analysis of the Álfafjörður dyke swarm: implications for shallow crustal magma transport in Icelandic volcanic systems. in *The Use of Palaeomagnetism and Rock Magnetism to Understand Volcanic Processes*, Vol. **396**, pp. 107–132, eds Ort, M.H., Porreca, M. & Geissman, J.W., Geological Society Special Publications, The Geological Society of London.
- Ernst, R.E. & Baragar, W.R.A. 1992. Evidence from magnetic fabric for the flow pattern of magma in the Mackenzie giant radiating dyke swarm, *Nature*, **356**, 511–513.
- Féménias, O., Diot, H., Berza, T., Gauffriau, A. & Demaiffe, D., 2004. Asymmetrical to symmetrical magnetic fabric of dikes: Paleo-flow orientations and Paleo-stresses recorded on feeder-bodies from the Motru Dike Swarm (Romania), *J. Struct. Geol.*, **26** (8), 1401–1418.

- Geoffroy, L., Callot, J.P., Aubourg, C. & Moreira, M., 2002. Magnetic plagioclase linear fabric discrepancy in dikes: a new way to define the flow vector using magnetic foliation, *Terra Nova*, **14**(3): 183–191.
- Hargraves, R.B., Johnson, D. & Chan, C.Y., 1991. Distribution anisotropy: the cause of AMS in igneous rocks? *Geophys. Res. Lett.*, **18**, 2193–2196.
- Harrison, R. J. & Feinberg, J. M., 2008. FORCinel: an improved algorithm for calculating first-order reversal curve distributions using locally weighted regression smoothing, *Geochem. Geophys. Geosyst.*, **9**, Q05016, doi:10.1029/2008GC001987.
- Hastie, W.W., Aubourg, C. & Watkeys, M.K., 2011. When an inverse fabric is not inverse: an integrated AMS-SPO study in MORB-like dykes, *Terra Nova*, **23**, 49–55.
- Herrero-Bervera, E., Walker, G.P.L., Cañón-Tapia, E. & Garcia, M.O., 2001. Magnetic fabric and inferred flow direction of dikes, conesheets and sill swarms, Isle of Skye, Scotland, *J. Volc. Geotherm. Res.*, **106**(3–4), 195–210.
- Hrouda, F., 2002. The use of anisotropy of magnetic remanence in the resolution of the anisotropy of magnetic susceptibility into its ferromagnetic and paramagnetic components, *Tectonophysics*, **347**, 269–281.
- Hrouda, F. & Ježek, J., 2014. Frequency-dependent AMS of rocks: a tool for the investigation of the fabric of ultrafine magnetic particles. *Tectonophysics*, **629**, 27–38.
- Ildefonse, B., Launeau, P., Bouchez, J.L. & Fernandez, A., 1992. Effect of mechanical interactions on the development of shape preferred orientations: a two-dimensional experimental approach, *J. Struct. Geol.*, **14**, 73–83.
- Jackson, M., 1991. Anisotropy of magnetic remanence: a brief review of mineralogical sources, physical origins and geological applications, and comparison with susceptibility anisotropy, *PAGEOPH*, **136**, 1–28.
- Jeffery, G.B., 1922. The motion of ellipsoidal particles immersed in a viscous fluid, *Proc. R. Soc. Lond., A*, **102**, 161–179.
- Jelinek, V., 1977. *The Statistical Theory of Measuring Anisotropy of Magnetic Susceptibility of Rocks and its Application*, Geophysika, Brno, pp. 1–88.
- Khan, M.A., 1962. The anisotropy of magnetic susceptibility of some igneous and metamorphic rocks, *J. geophys. Res.*, **67**, 2873–2885.
- Kissel, C., Laj, C., Sigurdsson, H. & Guillou, H., 2010. Emplacement of magma in Eastern Iceland dikes: insights from magnetic fabric and rock magnetic analyses, *J. Volc. Geotherm. Res.*, **191**, 79–92.
- Knight, M.D. & Walker, G.P.L., 1988. Magma flow directions in dikes of the Koolau Complex, Oahu, determined from magnetic fabric studies, *J. geophys. Res.*, **93**(B5): 4301–4319.
- Lowrie, W., 1990. Identification of ferromagnetic minerals in a rock by coercivity and unblocking temperature properties, *Geophys. Res. Lett.*, **17**, 159–162.
- McCabe, C.M., Jackson, M & Ellwood, B.B., 1985. Magnetic anisotropy in the Trenton limestone: results of a new technique, anisotropy of anhysteretic susceptibility. *Geophys. Res. Lett.*, **12**, 333–336.
- Moore, J.G. & Lockwood, J.P., 1973. Origin of comb layering and orbicular structure, Sierra Nevada Batholith, California, *Geol. Soc. Am. Bull.*, **84**, 1–20.
- Muxworthy, A.R. & Williams, W., 2009. Critical superparamagnetic/single-domain grain sizes in interacting magnetic particles: implications for magnetosome crystals. *J. R. Soc. Inter.*, **6**(41), 1207–1212.
- Muxworthy, A.R., Heslop, D. & Williams, W., 2004. Influence of magnetostatic interactions on first-order-reversal-curve (FORC) diagrams: a micromagnetic approach. *Geophys. J. Int.*, **158**, 888–897.
- Muxworthy, A.R., King, J.G. & Heslop, D., 2005. Assessing the ability of first-order reversal curve (FORC) diagrams to unravel complex magnetic signals, *J. geophys. Res.*, **110**, B01105, doi:10.1029/2004JB003195.
- Néel, L., 1949. Théorie du trainage magnétique des ferromagnétiques au grains fin avec applications aux terres cuites, *Ann. Geophys.*, **5**, 99–136.
- Nicolas, A., 1992. Kinematics in magmatic rocks with special reference to gabbros, *J. Petrol.*, **33**, 891–915.
- Pike, C.R., Roberts, A.P. & Verosub, K.L., 2001. First-order reversal curves diagrams and thermal relaxation effects in magnetic particles, *Geophys. J. Int.*, **145**, 721–730.
- Poland, M.P., Fink, J.H. & Tauxe, L., 2004. Patterns of magma flow in segmented silicic dikes at Summer Coon volcano, Colorado: AMS and thin section analysis, *Earth planet. Sci. Lett.*, **219**, 155–169.
- Porreca, M., Acoella, V., Massimi, E., Mattei, M., Funciello, R. & De Benedetti, A.A., 2006. Geometric and kinematic features of the dike complex at Mt. Somma, Vesuvio (Italy), *Earth planet. Sci. Lett.*, **245** (1–12): 389–407.
- Potter, D.K. & Stephenson, A., 1988. Single-domain particles in rocks and magnetic fabric studies, *Geophys. Res. Lett.*, **15**, 1097–1100.
- Raposo, M.I.B. & D'Agrella-Filho, M.S., 2000. Magnetic fabrics of dike swarms from SE Bahia State, Brazil: their significance and implications for Mesoproterozoic basic magmatism in the Sao Francisco Craton, *Pre-cambrian Res.*, **99**(3–4): 309–325.
- Roberts, A.P. & Pillans, B.J., 1993. Rock magnetism of Lower/Middle Pleistocene marine sediments, Wanganui Basin, New Zealand, *Geophys. Res. Lett.*, **20**, 839–842.
- Roberts, A.P., Pike, C.R. & Verosub, K.L., 2000. First-order reversal curve diagrams: a new tool for characterizing the magnetic properties of natural samples, *J. geophys. Res.*, **105**, 28,461–28,475.
- Rochette, P., Jackson, M. & Aubourg, C., 1991. Rock magnetism and the interpretation of anisotropy of magnetic susceptibility, *Rev. Geophys.*, **30**, 209–226.
- Rochette, P., Aubourg, C. & Perrin, M., 1999. Is this magnetic fabric normal? A review and case studies in volcanic formations, *Tectonophysics*, **307**, 219–234.
- Smirnov, A.V., 2006. Low-temperature magnetic properties of magnetite using first-order reversal curve analysis: implications for the pseudo-single-domain state, *Geochem. Geophys. Geosyst.*, **7**, Q11011, doi:10.1029/2006GC001397.
- Soriano, C., Beamud, E. & Garcés, M., 2007. Dike intrusion under shear stress: effects on magnetic and vesicle fabrics in dikes from rift zones of Tenerife (Canary Islands), *J. Struct. Geol.*, **29**, 1931–1942.
- Soriano, C., Beamud, E. & Garcés, M., 2008. Magma flow in dikes from rift zones of the basaltic shield of Tenerife, Canary Islands: implications for the emplacement of buoyant magma, *J. Volc. Geotherm. Res.*, **173**, 55–68.
- Stephenson, A., 1994. Distribution anisotropy: two simple models for magnetic lineation and foliation, *Phys. Earth planet. Inter.*, **82**, 49–53.
- Tauxe, L., 2010. *Essentials of Paleomagnetism*, University of California Press Ltd., 489 pp.
- Tauxe, L., Mullender, T.A.T. & Pick, T. 1996. Potbellies, wasp-waists, and superparamagnetism in magnetic hysteresis, *J. geophys. Res.*, **101**, 571–583.
- Tauxe, L., Gee, J.S. & Staudigel, H., 1998. Flow directions in dikes from anisotropy of magnetic susceptibility data: the bootstrap way, *J. geophys. Res.*, **103**(B8), 17 775–17 790.
- Till, J.L., Jackson, M.J., Rosenbaum, J.G. & Solheid, P., 2011. Magnetic properties in an ash flow tuff with continuous grain size variation: a natural reference for magnetic particle granulometry, *Geochem. Geophys. Geosyst.*, **12**, Q07Z26, doi:10.1029/2011GC003648.
- Walderhaug, H., 1993. Rock magnetic and magnetic fabric variations across three thin alkaline dykes from Sunnhordland, Western Norway: influence of initial mineralogy and secondary chemical alterations, *Geophys. J. Int.*, **115**, 97–108.
- Worm, H-U. & Jackson, M., 1999. The superparamagnetism of the Yucca Mountain Tuff, *J. geophys. Res.*, **104**, 25 415–25 425.

## SUPPORTING INFORMATION

Additional Supporting Information may be found in the online version of this paper:

**Suppl. file #1.** Selection of hysteresis loops of samples from dike profiles. (<http://gji.oxfordjournals.org/lookup/suppl/doi:10.1093/gji/ggv495/-/DC1>).

Please note: Oxford University Press is not responsible for the content or functionality of any supporting materials supplied by the authors. Any queries (other than missing material) should be directed to the corresponding author for the paper.